NASA
Technical
Paper
2255

March 1984

Steady Internal Flow and Aerodynamic Loads Analysis of Shuttle Thermal Protection System

Dennis H. Petley,
William Alexander, Jr.,
George W. Ivey, Jr.,
and Patricia A. Kerr

NASA

NASA Technical Paper 2255

1984

Steady Internal Flow and Aerodynamic Loads Analysis of Shuttle Thermal Protection System

Dennis H. Petley,
William Alexander, Jr.,
George W. Ivey, Jr.,
and Patricia A. Kerr

Langley Research Center
Hampton, Virginia

National Aeronautics
and Space Administration

Scientific and Technical Information Branch

CONTENTS

SUMMARY 1

INTRODUCTION 1

SYMBOLS 1

INTERNAL FLOW MODEL USING MITAS 4
Modeling of Conductance 5
Discussion of Parameters Which Influence Flow in TPS 9

FORCE AND MOMENT MODEL 11
Normal Forces and Moments 11
Gap Forces and Moments 12
Skin-Friction Forces and Moments 14

RESULTS AND DISCUSSION 15
Comparison With Test Data 15
Parametric Runs of Multitile Model 15

CONCLUDING REMARKS 17

APPENDIX - EQUATIONS FOR HEAT TRANSFER AND FLUID FLOW 18

REFERENCES 20

FIGURES 21

SUMMARY

An analytical model for calculation of ascent steady-state tile loading was developed and validated with wind-tunnel data. The analytical model is described and results are given. Results are given for loading due to shocks and skin friction. The analysis included calculation of internal flaw (porous media flow and channel flow) to obtain pressures and integration of the pressures to obtain forces and moments on an insulation tile. A heat-transfer program was modified by using analogies between heat transfer and fluid flow so that it could be used for internal-flow calculation. The type of insulation tile considered was undensified reusable surface insulation (RSI) without gap fillers, and the location studied was the lower surface of the orbiter. Force and moment results are reported for parameter variations on surface pressure distribution, gap sizes, insulation permeability, and tile thickness.

INTRODUCTION

The NASA Structures Team was established in February 1980 for the purpose of resolving problems of the Shuttle Thermal Protection System (TPS) as they existed at that time. This work was performed to support the NASA Structures Team in the independent structural assessment of the TPS for the first launch of the Space Transportation System (STS-1). The present analysis of TPS steady aerodynamic ascent loads was needed because the existing analysis did not agree with wind-tunnel data. The purpose of this report is to describe the detailed analysis which was done at the Langley Research Center (LaRC) and to present some selected results. The analysis was accomplished by formulating a mathematical model for calculations of steady aerodynamic loads by adapting the Martin Marietta Interactive Thermal Analysis System to perform internal steady flow analysis. The MITAS (ref. 1) program could be used for internal-flow calculation by modifying the input to the program based on analogies between heat transfer and fluid flow. The program was used to calculate internal mass flows and pressures of an array of nine LI900 undensified tiles (9 lb/ft^3 density). A postprocessor loads calculation program was written to calculate loads using output from the MITAS program and other inputs. This model was used to calculate tile loads caused by stationary shocks.

This report consists of sections on flow modeling and validation, force and moment postprocessor, and results of parametric runs. A program user guide and a copy of the MITAS input computer code of the model are available in reference 2. This computer model was subsequently modified for use in gap heating analysis (described in ref. 3).

SYMBOLS

ΔA tile area on which shear stress acts, in^2

A_c cross-sectional area for flow, in^2

A_{el} tile element area, in^2

A_p	area on which pressure difference acts, in^2
A_σ	area which is stressed, in^2
C_d	discharge coefficient
C'_f	local skin-friction coefficient
D_{tile}	tile thickness, in.
F	force, lbf
F_X	force in the x-direction, lbf
F_Y	force in the y-direction, lbf
F_Z	force in the z-direction, lbf
G	conductance for heat transfer, Btu/hr-°F; conductance for fluid flow, lbm/sec-psi
g_c	mass unit conversion, $lbm-ft/lbf-sec^2$
H	length of moment arm, in.
K_p	permeability, in^2
K_r	tile roughness factor, in.
K_s	spring constant, lbf/in.
k	thermal conductivity, Btu/hr-ft-°F
L	length of tile diagonal, 8.49 in.
ℓ_1	SIP height after tile installation, in.
ℓ_2	filler-bar thickness after tile installation, in.
M	moment, in-lbf
m	mass-flow rate, lbm/sec
P	pressure, psi
Δp	pressure difference, psi
Δp_1	pressure difference between surface and SIP, psi
Δp_2	pressure difference between tile gap and filler bar, psi
p_{GB}	pressure at bottom of gap, psi
p_{GT}	pressure at top of gap, psi

p_{sur}	pressure on tile surface, psi
p_{TBL}	pressure at tile bond line, psi
$\dot{q}$	heat-flow rate, Btu/hr
ΔS	distance from center of one node to next, in.
T	temperature, °R
TBL	tile bond line
U_∞	free-stream velocity, fps
W_{el}	tile element width, in.
W_f	width of gap between filler bar and tile
W_{min}	minimum gap between filler bar and tile
W_o	initial gap width
W_t	width of gap between tiles
W_{tile}	tile width, in.
X,Y,Z	Shuttle axis system
X_l, Y_l, Z_l	local (tile) axis system
x	distance from airfoil leading edge, in. (fig. 13)
Δx	streamwise integration step, in.
x'	distance from shock, $x - x_{shock}$, in. (fig. 13)
x_l, y_l, z_l	local (tile) coordinate system
x_o	distance from airfoil leading edge to tile leading edge, in. (fig. 13)
x_s	distance from tile leading edge to foot of shock, in.
x_{shock}	distance from airfoil leading edge to shock location, in. (fig. 13)
y	distance along Y-axis with respect to Shuttle coordinate system
δ	boundary-layer thickness, in.
μ	viscosity, lbm/in-sec
μ_∞	viscosity of free stream, lbm/ft-sec
ρ	density, lbm/in3
ρ_∞	free-stream density, lbm/ft^3

τ_w surface shear stress unaccounted for shock, lbf/ft^2

$\bar{\tau}_w$ surface shear stress accounted for shock, lbf/ft^2

Subscripts:

i,j tile matrix location

l local (tile)

X x-direction

Y y-direction

Z z-direction

INTERNAL FLOW MODEL USING MITAS

A three-dimensional analytical model of an array of nine LI900 undensified tiles was developed to adequately represent the internal flow through the Shuttle thermal protection system. The primary requirement was to obtain pressures in the tile and in the gaps between tiles in sufficient detail to allow tile loading to be determined. MITAS (ref. 1) was used in preference to writing a custom computer program to save time and manpower. MITAS (Martin Marietta Interactive Thermal Analysis System) is a general purpose finite-difference heat-transfer program and was applicable to this analysis of internal incompressible (low subsonic Mach number) flow because of the similarity in the equations for internal incompressible flow and the equations for heat transfer.

The first step in the modeling was to establish in detail how the MITAS program would be used to model incompressible internal flow. The Laplace equation is applicable to both incompressible flow and heat transfer. These types of problems can be converted to an analog representation consisting of nodes connected by conductors, which is precisely the way in which MITAS is used to represent a heat-transfer problem. This type of representation - commonly called a lumped node, electrical analog representation of a heat-transfer problem - also applies to internal incompressible flow. The required input to the MITAS program is the description of nodes and conductors for the electrical analog representation of the thermal or fluid flow problem. MITAS could be used directly for this flow problem because of the exact correspondence between pressure and temperature and between mass flow and heat flaw, Some comparisons of conductors for heat flow and fluid flow are given in the appendix.

The input to the MITAS program for the steady-state flow situation is first of all the node and conductor definition for the electrical analog representation of the geometric configuration. The network and corresponding MITAS input was first developed for a single tile; then with the single-tile representation as a guide, the network for the multiple-tile model was developed. Three-dimensional modeling was required to obtain internal pressure for tile, strain isolation pad (SIP), and filler-bar and tile-to-tile gap pressures from given surface pressure boundary conditions.

A single-tile three-dimensional model was developed first. A sketch showing the flow paths through a single tile is shown in figure 1. The ceramic coating which

covers most of the tile surface is assumed to be impermeable. Flow through cracks and chipped areas was neglected. The flow through the silicone rubber bond line on the bottom of the tile was also considered to be insignificant. Thus, areas where flow can enter or leave a tile are the terminator gap area and the 1/2-in-wide unbonded area on the bottom outer edge of the tile. Flow can enter or leave the SIP through the unbonded area on the bottom of the tile or the gap between the tile bottom and the filler bar, The connections to the surface through which all internal flow enters or leaves are the gaps between the tiles. With the flow paths in the TPS established, the next step was to define the nodes and conductors for the single-tile model. The dimensions of the single-tile model are 6 by 6 in., and the thickness of the tile and SIP are variable. The SIP thickness was set at 0.16 in. in this analysis. The nodal arrangement for the subject tile is shown in figures 2 through 4. Nodes 61 through 96, which are the nodes inside the tile at the surface, are shown in figure 2. Nodes 25 through 60 (inside the tile at the bond line plane), nodes G1 through G24 (at the bottom of the gap between tiles), and nodes B201 through B224 (the boundary nodes for the internal flow which are located at the surface over the gap between tiles) are shown in figure 3. Nodes 97 through 132, which are in the SIP, are shown in figure 4. Conductors were defined to connect the nodes in three dimensions. Examples of nodes in the x_1-y_1 plane that were connected by conductors would be 61 to 62, 61 to 67, 25 to 26, 25 to 31, 97 to 98, and 97 to 103. Examples of nodes that were connected by conductors for flow in the z_1-direction would be 61 to 25, 62 to 26, 67 to 31, 68 to 32, 25 to 97, 26 to 98, 31 to 103, and 32 to 104. There are two parallel flow paths from the bottom of the gap to the bottom of the tile: one flow path through the edge of the tile and one flow path under the edge of the tile between the tile and filler bar. (See fig. 1, view A.) These flow paths are represented in figure 3 with electrical resistance symbols connecting gap nodes to tile bond line nodes such as nodes G2 and 26, for example. Figure 3 also shows the conductors connecting surface boundary nodes to nodes at the bottom of the gap, such as the conductor shown connecting boundary node B202 to gap node G2.

With the single-tile model as a guide, a model of an array of nine tiles was developed by adding eight more similar tiles to the single-tile model. Flow from one tile to another is through the filler bar and through the gaps between tiles. The overall pattern of tiles for the multitile model is shown in figure 5. A staggered pattern was chosen because this is the dominant pattern of tiles on the Shuttle. The nine tiles in the model are shown numbered 1 through 9. Tile 9 is the subject tile, also referred to as the "0000" tile in figures 6, 7, and 8. The locations of the nodes in the multiple-tile array are shown in figures 6, 7, and 8. Figure 6 shows nodes inside the tile at the surface for each of the nine tiles. Figure 7 shows nodes at the tile bond line and at the surface and bottom of the adjacent gaps for each of the tiles. Figure 8 shows nodes in the SIP for each of the tiles.

Modeling of Conductance

After defining the nodes and conductor connections for the nine-tile model, the conductance values for these conductors were determined. The general categories of conductance values to be determined were tile material, SIP material, gap between tiles, tile terminator gap, gap between tile and filler bar, and gap between filler bar and SIP.

The conductance for flow through tile and SIP material was based on flow through porous media (ref. 4). The conductance for flow through porous media as used in the analysis is determined as follows:

$$G = \frac{K_p \rho A_c}{\mu \Delta s}$$

The flow through the tile in the terminator gap location, the tile bond line node at the edge of the tile (node 55 in fig. 3, for example), was modeled as flow through porous media by using an equivalent flow area. This equivalent flow area was the average of the terminator gap area (the product of terminator gap width and node width) and the node cross-sectional area for flow (the product of $D_{tile}/2$ and node width).

The equations which represent laminar flow between parallel walls were used to represent flow in the gap between tiles. The validity of using these equations was demonstrated in reference 5 by comparison of the theoretical results for laminar flow between parallel walls to experimental data for flow in the gaps between tiles. The equations for mass flow and conductance, from reference 6, for laminar flow between parallel walls as used in the analysis are as follows:

$$\dot{m} = -\frac{1}{12} \frac{\rho W_t^2 A_c}{\mu} \frac{dp}{ds}$$

$$G = \frac{1}{12} \frac{\rho W_t^2 A_c}{\mu \Delta s}$$

where

W_t tile-to-tile gap width

A_c flow area, W_t × Gap length

$\frac{dp}{ds}$ pressure gradient

Δs distance from center of one node to next

As can be seen from the equation for flow conductance, the conductance varies as the cube of the gap width. Consequently, it was necessary to account for changes in gap width caused by forces on the tiles for the gap between tiles and the gap between filler bar and tile.

The gap size, and resulting conductance for flow through the gap between tiles, was calculated iteratively for tiles which had significant size forces on them due to gap pressures. These side forces result from the surface pressure gradient, such as the gradient due to a shock being positioned over a tile. The tiles which required gap variations to be considered were the tiles which had the shock positioned on them coinciding with the shock being positioned on the subject tile. Figure 9 shows the

gaps between tiles in the global model, which were allowed to vary. The calculations of tile deflection were done only on the subject tile, tile 9, and the gap deflections of the other tiles, tile 3 and tile 7, were set to the same values as the corresponding locations on the subject tile. All other gaps between tiles were fixed at the initial gap opening. Gap pressures on the sides of the subject tile were integrated to obtain a resultant side force in the x_l- and y_l-directions. Rotation of the tile about the 2,-axis being neglected, the translational motion of the subject tile was then obtained from a spring representation of the SIP according to the following equations:

$$\Delta x_l = \frac{F_X}{K_S}$$

$$\Delta y_l = \frac{F_Y}{K_S}$$

where

Δx_l	subject tile x_l-deflection
F_X	force in the x_l-direction
Δy_l	subject tile y_l-deflection
F_Y	force in the y_l-direction
K_S	lateral spring constant for SIP

The SIP lateral spring constant used in this analysis was 110 lbf/in. (ref. 7). The gaps shown solid in figure 9 decrease from the initial value by the tile deflection, whereas the gaps shown hatched increase. A limiting condition for gap closure is the effective gap which exists when the two nonsmooth surfaces are in contact. The gaps between tiles were adjusted based on the calculated pressures until the calculated gap sizes converged.

The gap size and resulting conductance for flow through the gap between tile and filler bar was calculated iteratively for all tiles in the global model. The size of this gap is determined by the relative normal deflection between the bottom surface of the tile edge and filler bar and also by a silicone rubber membrane effect. The size of this gap is determined by the pressure forces which act on the filler-bar membrane and tile, causing deflections from the initial position.

The dimensions and deflections which influence this gap are shown in figure 10. The equation which was used for this tile edge deflection due to stretching or compressing the SIP is

$$\Delta \ell_1 = \frac{\Delta p_1 A_{p1}}{E_1 A_{\sigma 1}} \ell_1$$

where

Δp_1 pressure difference between external surface and SIP

A_{p1} area on which Δp_1 acts, loading SIP

$A_{\sigma 1}$ area of SIP which is stressed

ℓ_1 SIP thickness after tile installation (0.16 in.)

E_1 modulus of elasticity for SIP

The filler-bar deflection is caused by the pressure differential across the silicone rubber surface membrane and is defined by

$$\Delta \ell_2 - \frac{\Delta p_2 A_{p2}}{E_2 A_{\sigma 2}} \ell_2$$

where

Δp_2 pressure difference between tile gap and filler bar

A_{p2} area of filler bar on which Δp_2 acts

A_{62} area of filler bar which is stressed

ℓ_2 filler-bar thickness after tile installation

modulus of elasticity for filler bar

The desired width of the gap between the filler bar (FB) and tile is obtained based on the following equation:

$$W_f = \Delta \ell_2 - \Delta \ell_1 + W_o$$

where

W_f width of gap between filler bar and tile

W_o initial gap width

A limiting condition for this gap width is

$$W_f \geq W_{min}$$

where W_{min} is the effective gap which exists when the tile edge touches the filler bar (0.001 in.). The final condition which was considered in the determination of the gap size was the silicone rubber membrane effect. This effect causes a check valve action which restricts flow out of the SIP/FB more than it restricts inflow.

It was assumed that this membrane effect would dominate the gap size determination such that for this analysis it was adequate to assume that the gap height for flow out of the SIP/FB would be w_{min} and the gap height for flow into the SIP/FB would be as calculated from the above equation for w_f. The gaps between the tile and filler bar and the resulting flow conductance based on laminar flow between parallel walls were also changed based on the calculated pressures until the calculated gaps converged.

Flow through the gap between the SIP and filler bar was modeled as flow through a slot. The discharge coefficient C_d for this slot was assumed to be 0.5. The flow crpss-sectional area for tiles with significant side deflections was varied consistent with the side deflections calculated for the deflections of the gap between tiles mentioned previously.

Discussion of Parameters Which Influence Flow in TPS

The parameters which influence flow in TPS can be grouped into the following categories:

1. Surface pressure distribution
2. Tile-to-tile gaps
3. Terminator gaps
4. Internal tile flow
5. Tile-to-SIP flow path
6. Gap between tile and filler bar
7. Internal SIP flow
8. Gap between SIP and filler bar

In each of these categories, all known parameters were evaluated to determine which ones were significant enough to be included in the flow model.

The first area to be discussed is the surface pressure distribution. The parameters which were considered for this category in the model in order of importance were shock strength, shock location, shock smearing, absolute pressure, and absolute temperature. Shock location was defined as the location of the foot of the shock on the tile, and shock strength was defined as the pressure difference between the foot and the peak. Shock smearing has to do with the distance over which the shock is spread, which is normally governed by boundary-layer thickness. Absolute temperature influences viscosity and density of gas, whereas absolute pressure produces mainly a density effect.

In the category of tile-to-tile gaps, the parameters considered were minimum gap width, initial gap width, SIP shear stiffness, tile thickness, and gap pattern. The initial gap occurs in the unloaded condition, whereas the minimum gap is the gap which represents tile-to-tile contact. SIP shear stiffness affects the side-force deflection characteristics of the tile; these side deflections are important in determining gap variations. The tile thickness and tile pattern affect the geometry

of these flow paths. The model was limited to one gap pattern: a staggered pattern of square tiles.

In the category of the terminator gap, the only parameter considered was the terminator gap width.

In the category of internal tile flow, the parameters considered were tile thickness and tile permeability.

In the category of tile-to-SIP flow path, the parameters considered were effect of tile side deflection on the flow path, dimensional tolerancing on the SIP and filler bar, and the tile to SIP discharge coefficient. The dimensional tolerancing, side deflections, and discharge coefficient describe the flow through the slot between the SIP and filler bar.

In the category of flow through the gap between the tile and filler bar, the parameters considered were membrane effects of the filler-bar silicone coating, initial gap size, SIP and filler-bar stiffness, and minimum gap effect. The membrane effect is a tendancy of the edge of the filler-bar coating to roll up against the bottom of the tile producing a checking effect on flow in the direction from the SIP to the gap between tiles. The same initial gap size and minimum gap size were specified for all tiles in the global model. The minimum gap size represents the condition where the edge of the tile is in contact with the filler-bar surface membrane. The stiffnesses of the SIP and filler bar were represented with an effective modulus of elasticity.

In the category of internal SIP flow, the parameters considered were SIP permeability, and SIP deflections. The permeability of the SIP was obtained from reference 6. These data had to be adjusted to account for differences between test conditions and expected flight conditions (the SIP expands under load in flight).

In the category of the gap between SIP and filler bar, which is a gap between the silicone membranes of the SIP and filler bar, the parameters considered were a discharge coefficient, the effect of tile side deflection, and the effect of dimensional tolerance.

The more significant categories in the model were surface pressure distribution, the gap between tile and filler bar, tile-to-tile gaps, and internal SIP flow. Less significant were the terminator gaps, internal tile flow, and tile-to-SIP flow path. The least significant category considered in the model was the gap between SIP and filler bar.

There are many other parameters influencing flow in TPS which were not considered significant enough to include in the flow model. Some relevant parameters which were not considered in the flow model, listed by category, are as follows:

1. Surface pressure distribution: shock stability and tile surface step effect

2. Tile-to-tile gaps: compressibility effects in the gaps, influence of tile rotations on gap size, and initial gap variation from tile to tile

3. Terminator gap: changes in tile porosity due to the coating application and gap machining process and variation of gaps from tile to tile

4. Internal tile flow: permeability of tile coating and bond line due to imperfections

5. Tile-to-SIP flow path: the effect of rotational deflections and z_1-deflections of the tile

6. Gap between tile and filler bar: condition of the filler-bar transfer coat edge, condition of the tile bottom surface, changes in filler bar and SIP caused by proof testing, and dimensional tolerance from tile to tile

7. Internal SIP flow: effect of proof testing, directional bias of SIP, and wicking of silicone rubber into the SIP

8. Gap between SIP and filler bar: dimensional variations from tile to tile and changes due to the bonding process

FORCE AND MOMENT MODEL

The force and moment model is a postprocessor routine of the overall MITAS tile flow analysis model. The force and moment model numerically integrates the pressure profiles produced by the MITAS model to determine the forces and corresponding moments on the Shuttle tiles. The model accounts for the pressure distributions across the tile surface, at the tile bond line, and at the top and bottom of the gap around the tile perimeter. The model also includes skin-friction effects. The analysis employs a right-hand coordinate system and resolves the forces and moments in the x-, y-, and z-directions (fig. 11).

The tile was separated into 1-in^2 elements producing a 6 × 6 matrix on the tile surface and at the tile bond line, and 24 elements in the gap around the tile perimeter (fig. 12). The pressures on the tile surface and at the tile bond line were assumed to be constant per element. In the gap, the pressure was assumed to follow a linear distribution from the top to the bottom of the gap at each station around the tile. The pressures on the tile surface and at the tile bond line contribute to the normal forces and the moments about the X- and Y-axes. The gap pressures around the tile perimeter contribute to the forces in the x- and y-directions and the moments about the X-, Y-, and Z-axes. The skin friction contributes to the force in the x-direction and moment about the Y-axis. The calculated forces and moments are added together to obtain the resultant vectors, F_X, F_Y, and F_Z and the resultant moments about the X-, Y-, and Z-axes, M_X, M_Y, and M_Z.

Normal Forces and Moments

With the use of the pressure distributions on the tile surface and tile bond line, the normal force F_Z acting on the tile is expressed per element by

$$F_{Z_{ij}} = \left(p_{TBL_{ij}} - p_{sur_{ij}}\right) A_{el_{ij}}$$

where $1 \leq i \leq 6$, $1 \leq j \leq 6$, and $A_{el_{ij}} = W_{el}^2$. Therefore, the resultant normal force can be expressed by the summation,

$$F_Z = \sum_{i=1}^{6} \sum_{j=1}^{6} F_{Z_{ij}}$$

The moments about the X- and Y-axes produced by the normal forces and summed per element are defined by

$$M_X = \sum_{i=1}^{6} \sum_{j=1}^{6} F_{Z_{ij}} \left(\frac{L}{2} - y_{ij} \right)$$

$$M_Y = \sum_{i=1}^{6} \sum_{j=1}^{6} F_{Z_{ij}} \left(\frac{L}{2} - x_{ij} \right)$$

where $y_{ij} = (i - j + 6)(0.7071)$ and $x_{ij} = (i + j - 1)(0.7071)$.

Gap Forces and Moments

In the gap around the tile perimeter, the perpendicular force on each elemental face, the moment, and the moment arm are defined by

$$F_i = \frac{p_{GT_i} - p_{GB_i}}{2} W_{el} D_{tile} - p_{GB_i} W_{el} D_{tile}$$

$$M_i = \frac{p_{GT_i} - p_{GB_i}}{3} W_{el} D_{tile}^2 + \frac{p_{GB_i} W_{el} D_{tile}^2}{2}$$

$$H_i = \frac{M_i}{F_i}$$

where $1 \leq i \leq 24$. The components in the x- and y-directions are defined by

$$F_{X_i} = \frac{S_X F_i}{1.414}$$

$$F_Y = \frac{S_Y F_i}{1.414}$$

$$M_X = -F_{Y_i} H_i$$

$$M_{Y_i} = F_{X_i} H_i$$

where $1 \leq i \leq 24$ and

$S_X = +1$ $\quad (1 \leq i \leq 6$ and $19 \leq i \leq 24)$

$S_X = -1$ $\quad (7 \leq i \leq 18)$

$S_Y = +1$ $\quad (13 \leq i \leq 24)$

$S_Y = -1$ $\quad (1 \leq i \leq 12)$

The moment about the **Z-axis** per element is expressed by

$$M_{Z_i} = F_i L_i$$

where

$$L_i = [3.5 - (i - j)]$$

and

$j = 0$ $\quad (1 \leq i \leq 6)$

$j = 6$ $\quad (7 \leq i \leq 12)$

$j = 12$ $\quad (13 \leq i \leq 18)$

$j = 18$ $\quad (19 \leq i \leq 24)$

and $1 \leq i \leq 24$. The resultant moment about the Z-axis due to the gap pressures is determined by the sum

$$M_Z = \sum_{i=1}^{24} M_{Z_i}$$

Skin-Friction Forces and Moments

The skin-friction contribution to the force and moment calculation is based on the aerodynamic loading on the tile. The local shear stress τ_w on the tile surface is determined by the typical equation

$$\tau_w = \frac{1}{2g_c} C_f' \rho_\infty u_\infty^2$$

where C_f' is the local skin-friction coefficient. The skin-friction coefficient is assumed to follow the resistance formula for a uniformly rough flat plate (ref. 6):

$$C_f' = \left(\frac{2.87 + 1.58 \log x}{K_r} \right)$$

which is valid when $10^2 \leq x/K_r \leq 10^6$. (See fig. 13.) The shear stress is then adjusted to $\bar{\tau}_w$ to account for local boundary-layer separation directly beneath a shock on a tile. This adjustment is accomplished by determining a shear-stress reduction factor $(\bar{\tau}_w / \tau_w)$ as a function of a shock location and the boundary-layer thickness (ref. 8). The boundary-layer thickness δ is estimated by the smooth plate equation (ref. 6):

$$\delta = -0.37x \left(\frac{\rho_\infty U_\infty x/12}{\mu_\infty} \right)^{-1.5}$$

Given the free-stream conditions (i.e., ρ_∞, μ_∞, and U_∞), the shock location and the running length x where $x_o \leq x \leq x_o + L$, the ratio x'/δ can be determined so that the factor $\bar{\tau}_w/\tau_w$ can be found (ref. 8). The shear stress, τ_w is then calculated and adjusted to $\bar{\tau}_w$ to account for a shock on a tile. The differential area on which $\bar{\tau}_w$ acts is determined by

$$AA = 2(x - x_o)\,\Delta x \qquad \left(x \leq x_o + \frac{L}{2} \right)$$

$$AA = 2(x_o - x + L)\,\Delta x \qquad \left(x > x_o + \frac{L}{2} \right)$$

The corresponding differential forces and moments are then determined by

$$\Delta F_X = \frac{\bar{\tau}_W \Delta A}{144}$$

$$\Delta M_Y = \Delta F_X D_{tile}$$

Thus, the forces and moments due to the skin friction are

$$F_X = \sum \Delta F_X$$

$$M_Y = \sum \Delta M_Y$$

RESULTS AND DISCUSSION

The results of the analysis which are presented herein are a validation of the model and the calculated loads for a range of parameters. The model was validated by comparing calculated pressures with measured pressures from wind-tunnel tests. The load sensitivities of eight different parameters were determined by calculating forces and moments for varying input data to the model.

Comparison With Test Data

The pressure calculations of the flow model were validated by comparison with test data. The OS36 (fig. 14) and OS55 (fig. 15) Shuttle tile wind-tunnel test data were used for comparison with calculations (refs. 10 and 11, respectively). The "OS" in the test designation stands for orbiter structural test. For the OS36 and OS55 tests, arrays of tiles mounted on SIP and equipped with pressure measurement instrumentation were placed in a wind tunnel and subjected to aerodynamic shock environments. The purpose of these tests was to observe damage and measure internal pressures caused by shocks. Figure 16 shows comparison between calculated and measured pressures at the tile bond line at the diagonal centerline for the OS36 wind-tunnel test. The pressure at the tile bond line is the pressure inside the tile adjacent to the silicone rubber bond which attaches the tile to SIP. The rectangle at the bottom of the plot indicates the location of the 6- by 6-in. tile which is at a 45° angle so that the overall length in the flow direction is 8.49 in. Comparison of calculated and measured pressures at the tile bond line for the OS55 wind-tunnel test, runs 4:4, 4:5, and 4:6 are presented in figures 17, 18, and 19. The results of the calculations were in good agreement with the measured data; therefore, the model could be used to calculate forces and moments on tiles for STS-1 and no additional wind-tunnel testing of tiles was needed.

Parametric Runs of Multitile Model

A series of runs of the model was made to determine the influence of tile parameters on tile steady aerodynamic loads due to shocks. The tile parameters which were examined for sensitivity with the aid of the model are

1. Initial tile-to-tile gap
2. Terminator gap width
3. Gap between filler bar and tile
4. SIP permeability
5. Tile permeability
6. Tile thickness
7. Pressure effect (altitude effect)
8. Boundary-layer thickness

Aerodynamic force and moment calculations were made for several different shock pressure profiles over a range of shock locations from the leading to the trailing edge of the subject tile.

The parameters were studied with estimated pressure profiles for the mid-fuselage zone 6 (MF-6) region of the Shuttle orbiter (fig. 20) and measured pressure profiles from the OS55 wind-tunnel test. The pressure profiles and results of the parametric analysis are shown in figures 21 through 27. Figure 21 shows estimated MF-6 pressure profiles for shocks of 2 psi and boundary-layer thicknesses of 2.5 and 5.0 in. High and low upstream pressures were considered, high being 5.4 psi and low being 1.8 psi. Figure 22 shows the forces and moments produced by the pressure profiles of figure 21 for tile thicknesses of 1.0 and 2.0 in. and for various initial tile-to-tile gaps. Estimated MF-6 pressure profiles for two specific tiles in this region for the STS-1 ascent condition are shown in figure 23. The first tile is tile 394020-272, 1.47 in. thick, and is referred to as tile A. The second tile is tile 394034-087, 1.0 in. thick, and is referred to as tile B. Forces and moments for a nominal configuration of tile A and tile B are shown in figure 24, and the effect of initial gap variations on force and moment is shown in figure 25. The calculated forces and moments for tile A for single parameter variations of terminator gap, gap between filler bar and tile, SIP permeability, and tile permeability are presented in figure 26. The calculated forces and moments for tile B for single parameter variations of terminator gap and filler bar to tile gap are shown in figure 27. The measured pressure profiles from the OS55 wind-tunnel test are shown in figure 28. The forces and moments produced by the OS55 pressure profile for single parameter variations of initial tile-to-tile gap and tile thickness are shown in figures 29 and 30.

Several of the parameters studied were found to have a very significant effect on the tile loading. The location of the foot of the shock and the steepness of the shock were found to be significant in all cases where these parameters were varied. An increase in upstream pressure from 1.8 to 5.4 psi, an increase of 3.6 psi in the pressure distribution, caused the maximum forces and moments to increase by approxi-

mately 50 percent as shown in figures 22(a) and (b). When the initial tile-to-tile gap was decreased from the nominal value of 0.050 to 0.015 in., the maximum normal force for the MF-6 high pressure profile was decreased by 30 percent as shown in figure 22(c). The separated shock cases plotted in figure 25 and OS55 pressure profile results plotted in figure 29 also show significant effects when the tile-to-tile gap is decreased from the nominal value of 0.05 in. SIP permeability has a strong effect on normal force, as shown in figure 26(e), when the SIP permeability was increased by a factor of 4 for the separated shock, MF-6 profile, the maximum normal force increased by a factor of 2. Tile thickness has a significant effect on loading as shown in figure 30. The highest combined loading is calculated for the case where the foot of the shock is located at $x_s/L = 0.73$.

CONCLUDING REMARKS

A model was developed to calculate steady aerodynamic loads for Shuttle tiles. The use of the MITAS heat-transfer program to calculate internal incompressible flow, flow through porous media, and channel flow was demonstrated. Calculated pressures at the tile bond line caused by aerodynamic shock on the tile surface were in good agreement with measured pressures at the tile bond line from wind-tunnel tests. The model was used to calculate forces and moments on TPS tiles for STS-1.

The results of the analysis were used by the NASA Structures Team to obtain tile loadings for the STS-1 flight of the Shuttle for conditions where wind-tunnel data were not available.

Langley Research Center
National Aeronautics and Space Administration
Hampton, VA 23665
January 26, 1984

APPENDIX

EQUATIONS FOR HEAT TRANSFER AND FLUID FLOW

For heat flow,

$$\dot{q} = kA_c \frac{dT}{ds}$$

$$G = \frac{kA_c}{As}$$

where

$\dot{q}$ heat flux

k thermal conductivity

$\frac{dT}{ds}$ temperature gradient

A_c cross-sectional area for flow

As distance from center of one node to next

For flow through porous media (ref. 11),

$$\dot{m} = \frac{K_p \rho A_c}{\mu} \frac{dP}{ds}$$

$$G = \frac{K_p \rho A_c}{\mu\, As}$$

where

$\dot{m}$ mass-flow rate

K_p permeability

μ viscosity

ρ density

$\frac{dP}{ds}$ pressure gradient

For flow through slots and orifices,

$$\dot{m} = C_d A_c (2\rho g_c/\Delta p)^{1/2} \Delta p$$

$$G = C_d A_c (2\rho g_c/\Delta p)^{1/2}$$

where

$\dot{m}$ mass-flow rate

C_d discharge coefficient

A_c flow area

ρ density

g_c mass unit conversion

Δp pressure difference

Units which are commonly used for heat-flow rate and for temperature can also be compared with the units for the corresponding mass-flow rate and pressure which were chosen for the fluid flow model. For the thermal model, common units are

$\dot{q}$ heat-flow rate, Btu/hr

T temperature, °F

G conductance, Btu/hr-°F

For the fluid flow model, the units chosen were

$\dot{m}$ mass-flow rate, lbm/sec

P pressure, psi

G conductance, lbm/sec-psi

REFERENCES

1. Martin Marietta Interactive Thermal Analysis System - MZTAS-11-NOS-FTN Version. User's Manual. Martin Marietta Data Systems, Apr. 1977.

2. Kerr, Patricia A.; and Petley, Dennis H.: User's Guide: Steady-State Aerodynamic-Loads Program for Shuttle TPS Tiles. NASA TM-85724, 1984.

3. Petley, D. H.; Smith, D. M.; Edwards, C. L. W.; and Carlson, A. B.: Analysis of Gap Heating Due to Stepped Tiles in the Shuttle Thermal Protection System. NASA TP-2209, 1983.

4. Lawing, Pierce L.; and Nystrom, Donna M.: Pressure Drop Characteristics for Shuttle Orbiter Thermal Protection System Components: High Density Tile, Low Density Tile, Densified Low Density Tile, and Strain Isolation Pad. NASA TM-81891, 1980.

5. Dwoyer, Douglas L.; Newman, Perry A.; Thames, Frank C.; and Melson, N. Duane: A Tile-Gap Flow Mode1 for Use in Aerodynamic Loads Assessment of Space Shuttle Thermal Protection System: Parallel Gap Faces. NASA TM-83151, 1981.

6. Schlichting, Hermann (J. Kestin, transl.): Boundary-Layer Theory, Sixth ed. McGraw-Hi11 Book Co., Inc. c.1968.

7. Sawyer, James Wayne; and Waters, William Allen, Jr.: Room Temperature Shear Properties of the Strain Isolation Pad for the Shuttle Thermal Protection System. NASA TM-81900, 1981.

8. Adamson, T. C., Jr.; Liou, M. S.; and Messiter, A. F.: Interaction Between a Normal Shock Wave and a Turbulent Boundary Layer at High Transonic Speeds. NASA CR-3194, 1980.

9. Marshall, B. A.: Space Shuttle HRSI Tile Tests OS36 and OS37 in the NASA/Ames Research 11x11-Foot and 9x7-Foot Wind Tunnels Using Test Fixtures 96-0 and 81-0 (OS36/37). NASA CR-167668, 1983.

10. Kingsland, R. B.: Aerodynamic Venting Characteristics Tests of Full-Scale Space Shuttle Model 81-0 HRSI TPS Tiles Under a Simulated Launch Environment in the NASA/ARC 9x7-Foot Wind Tunnel (OS55 and OS57). NASA CR-167674, 1983.

11. Parker, Jerald D.; Boggs, James H.; and Blick, Edward F.: Introduction to Fluid Mechanics and Heat Transfer. Addison-Wesley Pub. Co., Inc., c.1969.

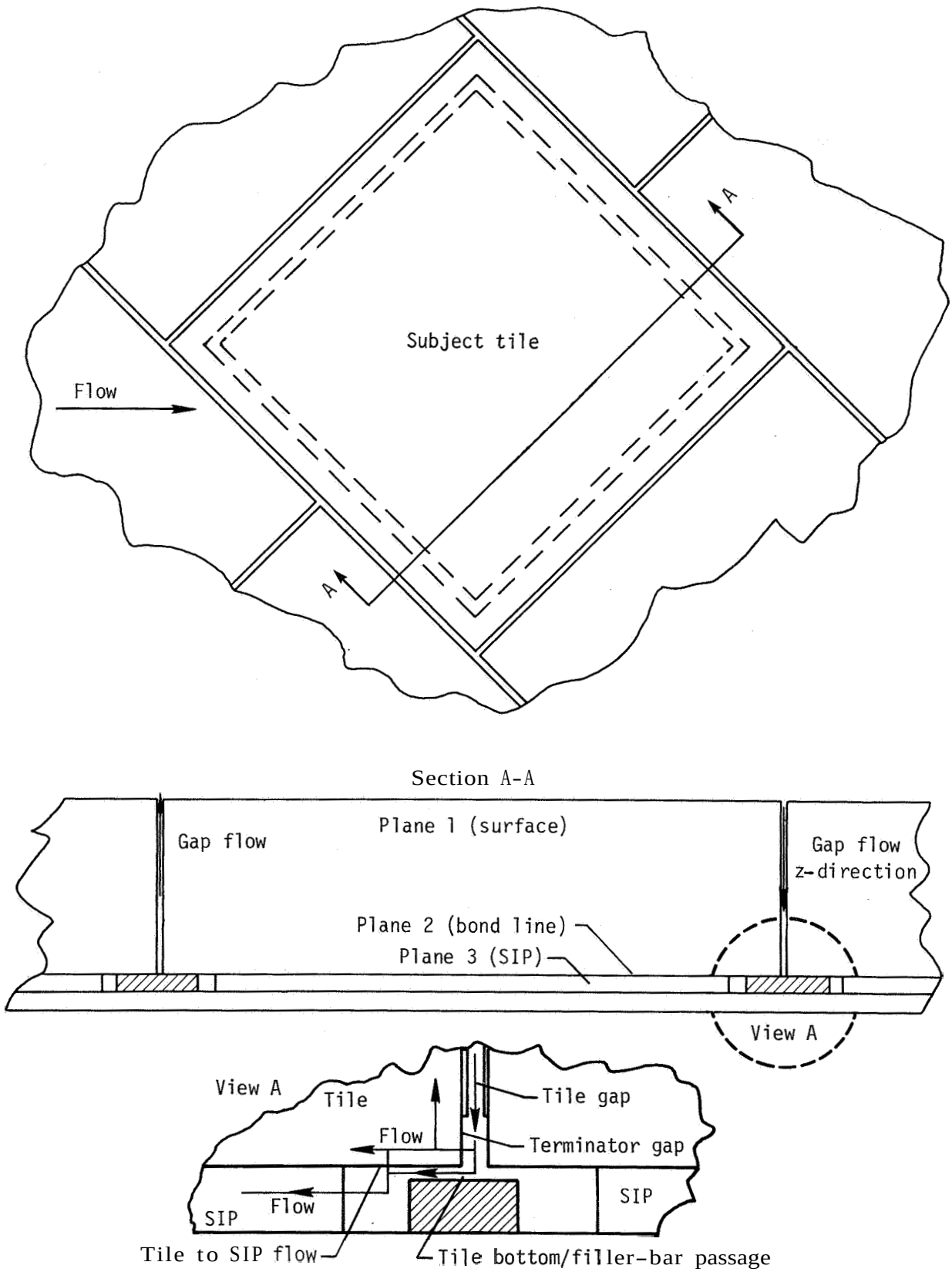

Figure 1.– Shuttle single-tile flow model.

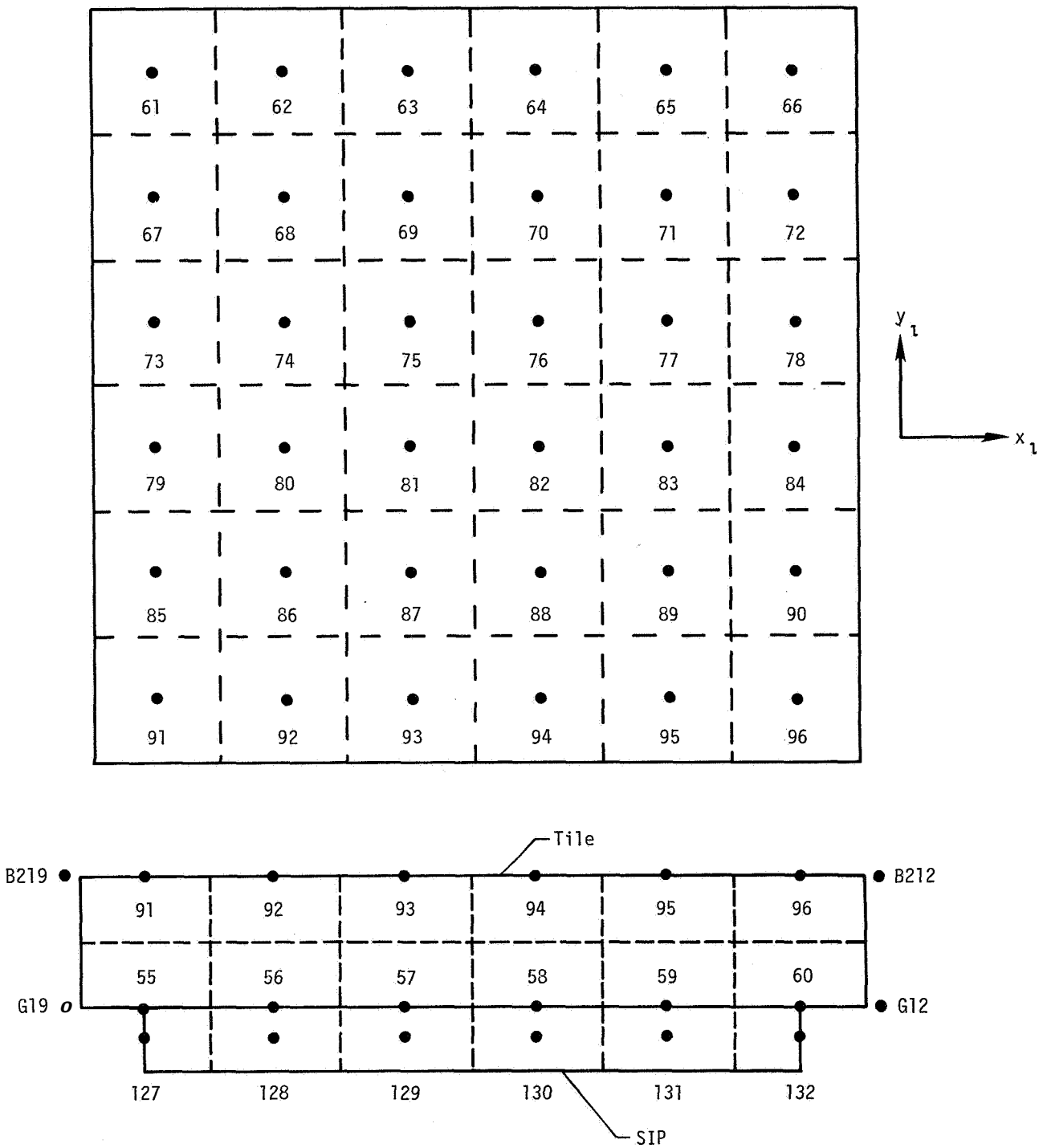

Figure 2.– **Subject** tile showing nodes inside tile **at** surface.

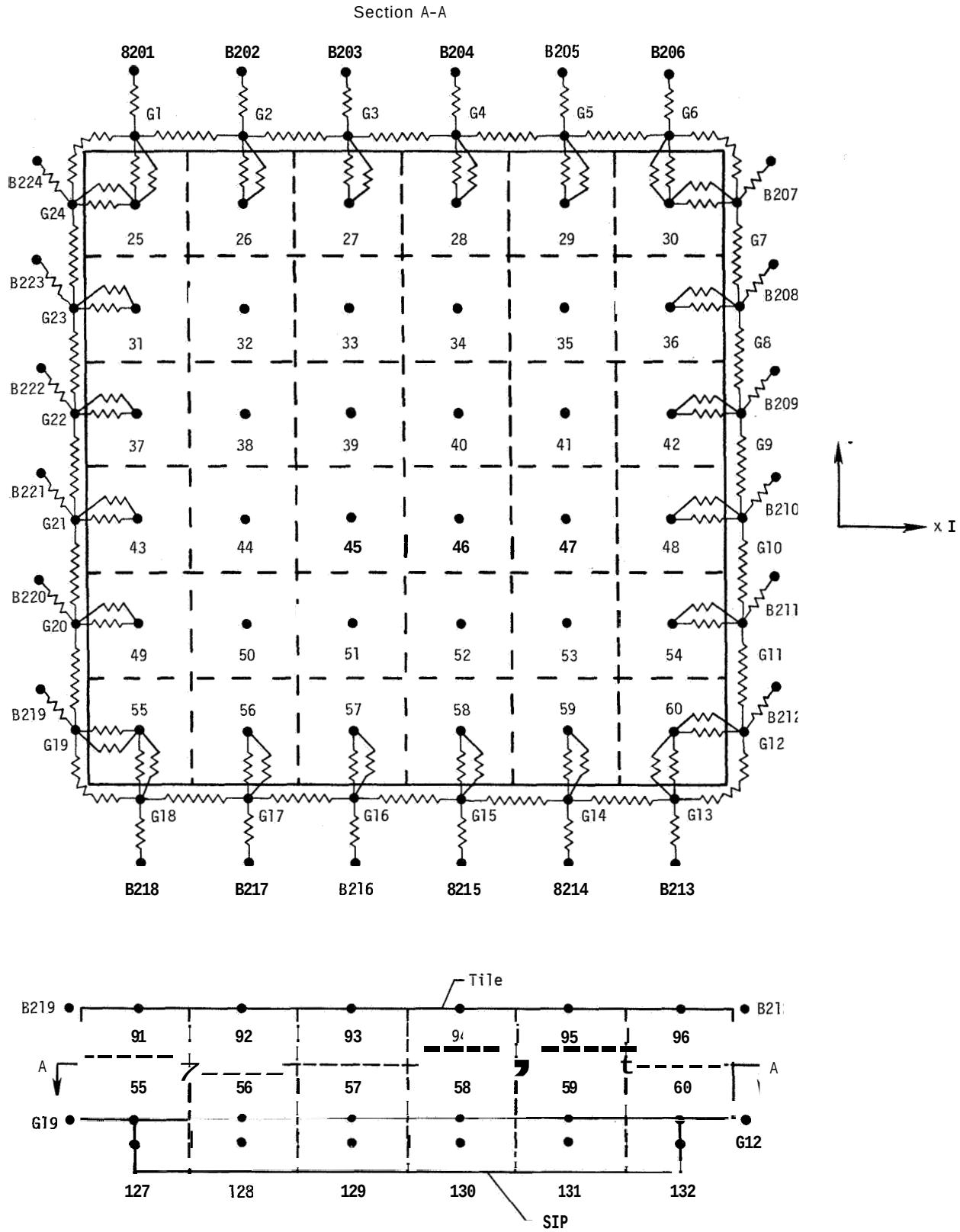

Figure 3.- **Subject tile** showing **nodes at** tile **bond** line.

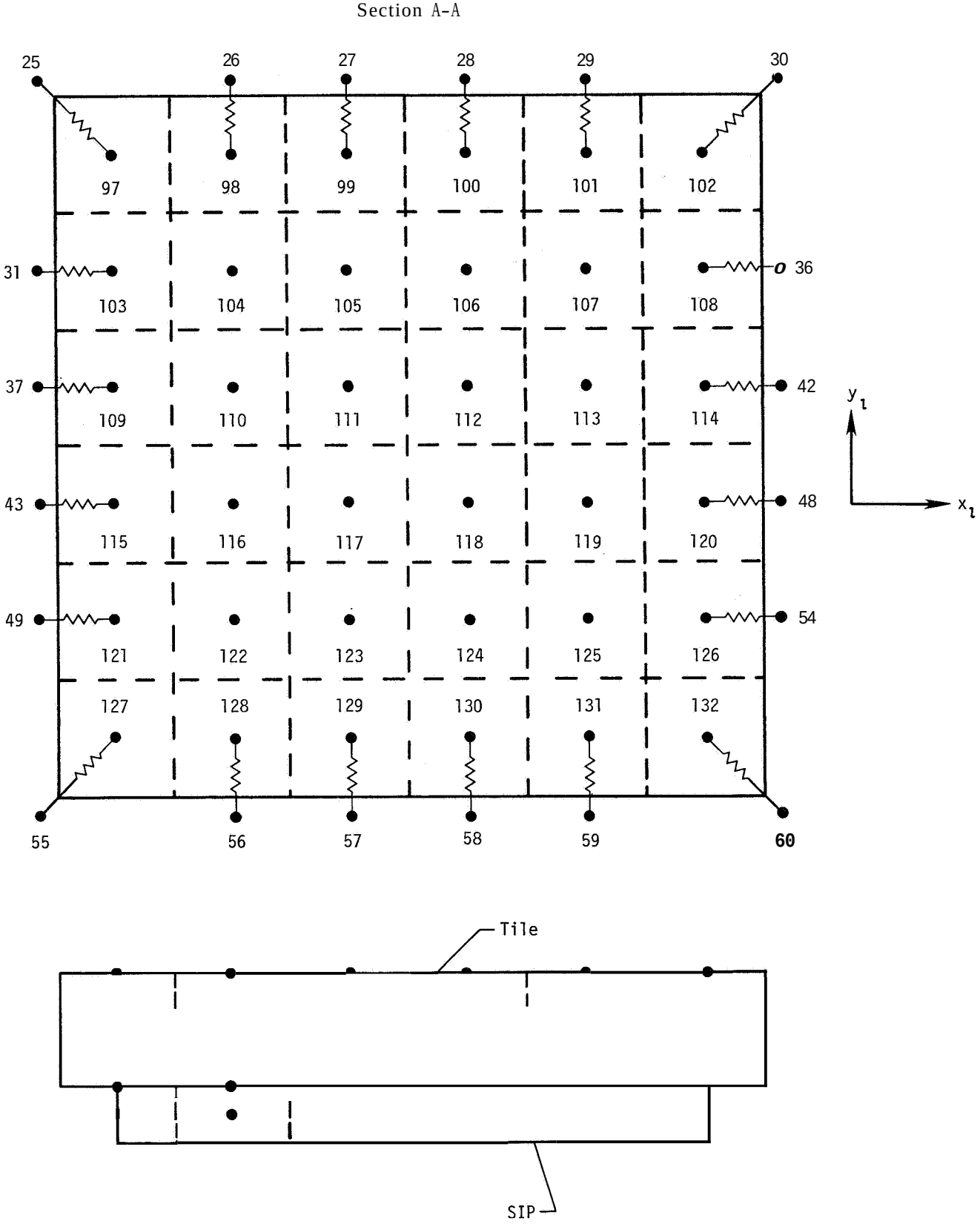

Figure 4.– **Subject** tile showing nodes in SIP.

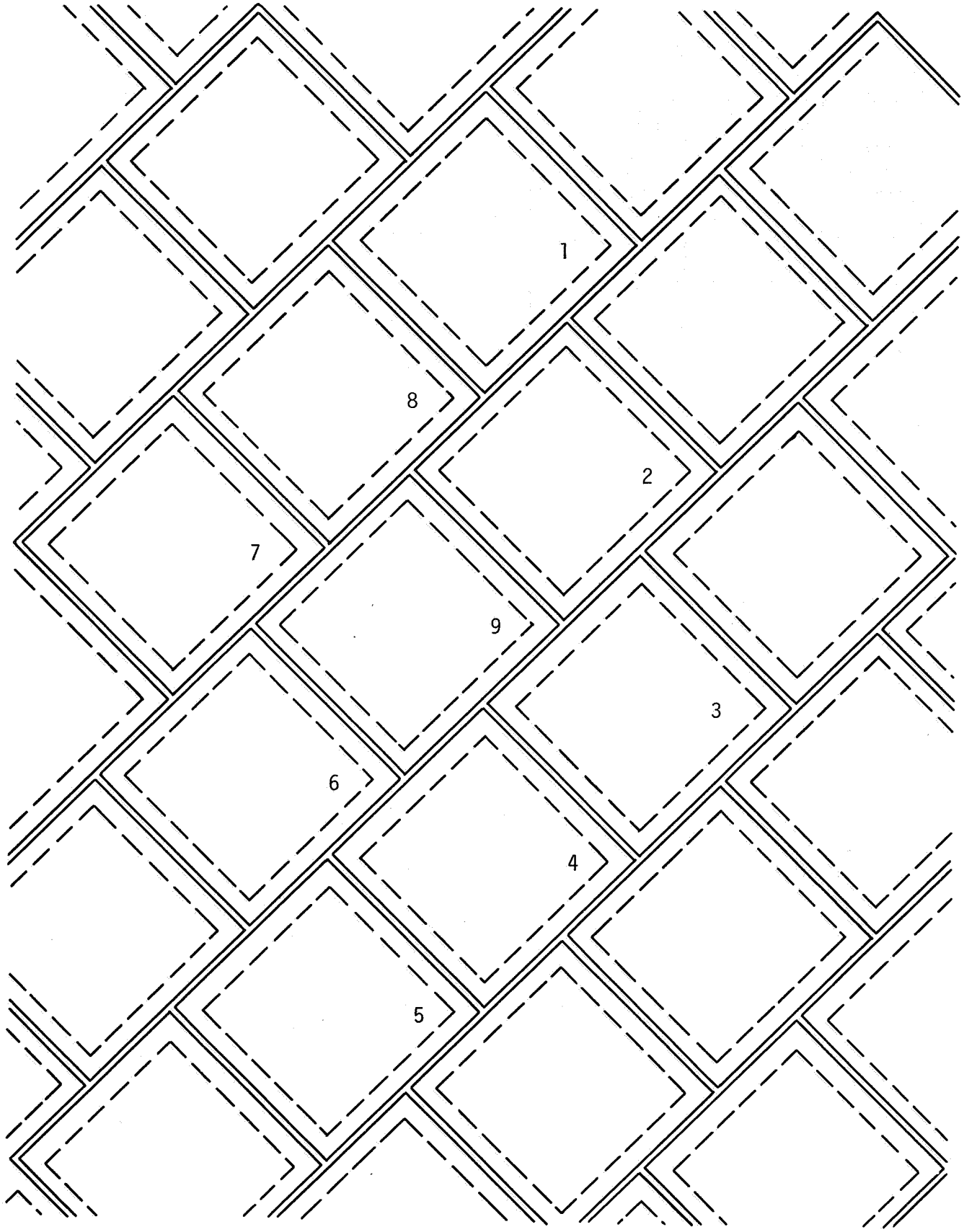

Figure 5.– Nine–tile array.

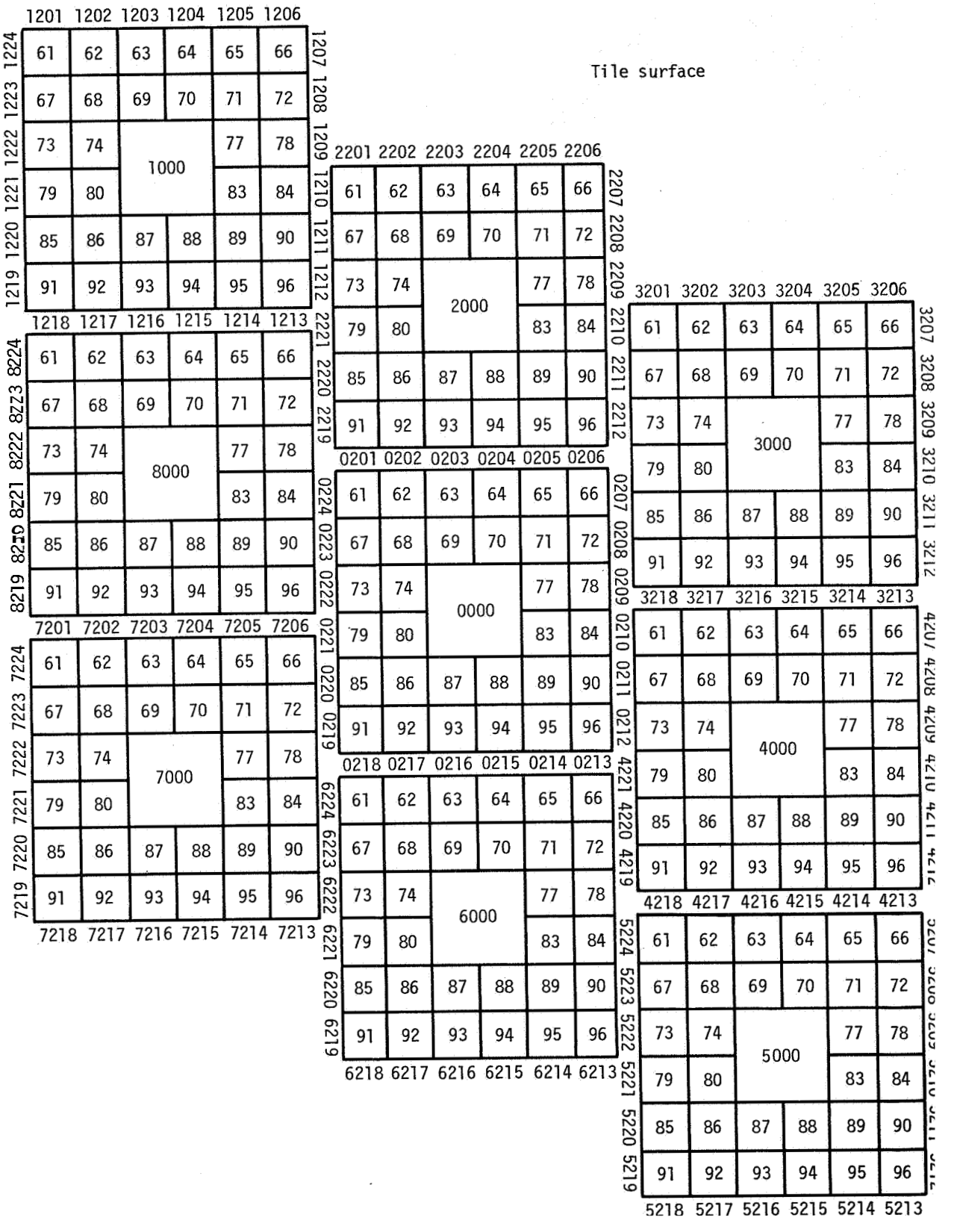

Figure 6.- Tile array showing surface nodes.

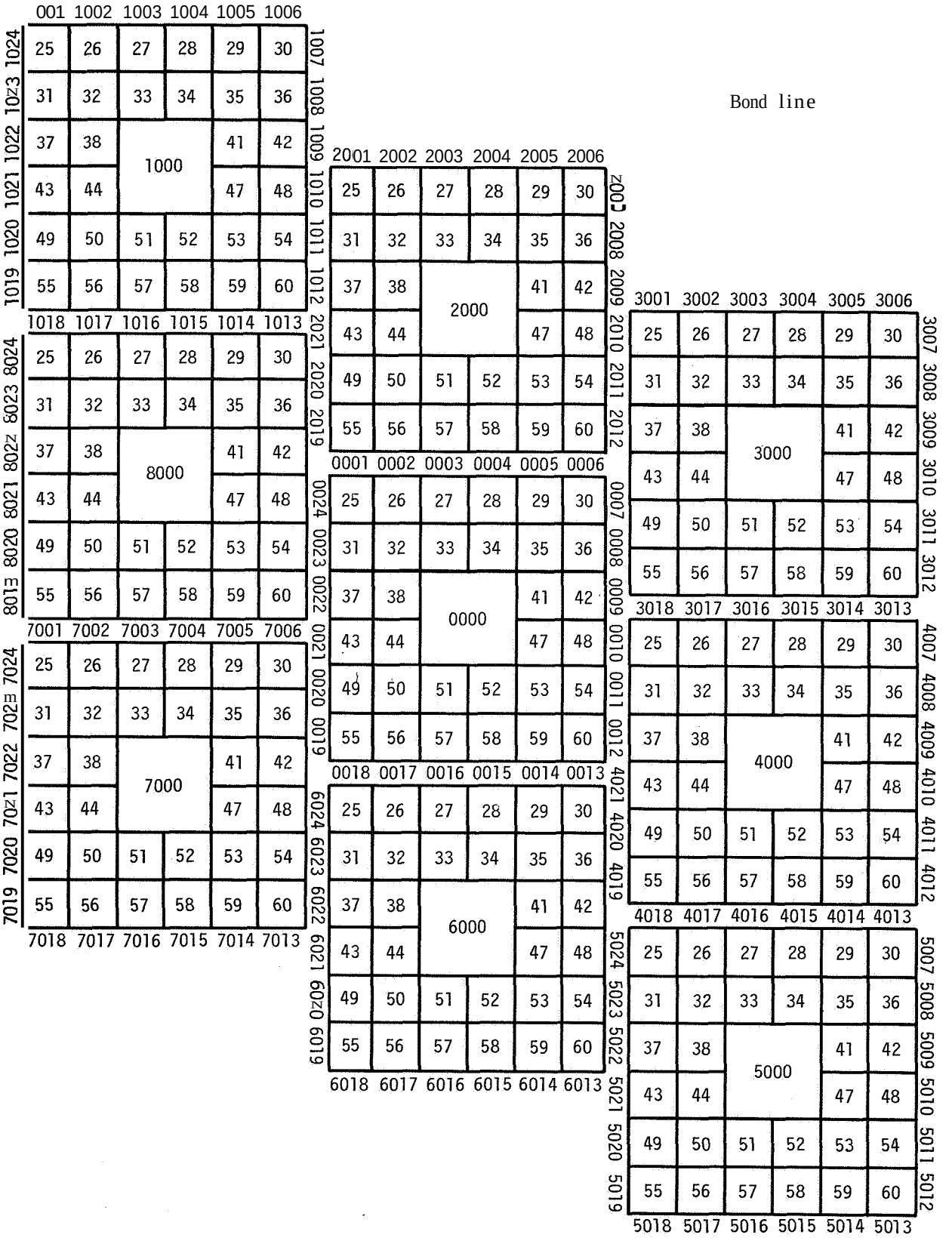

Figure 7.– Tile array showing nodes *at* bond line.

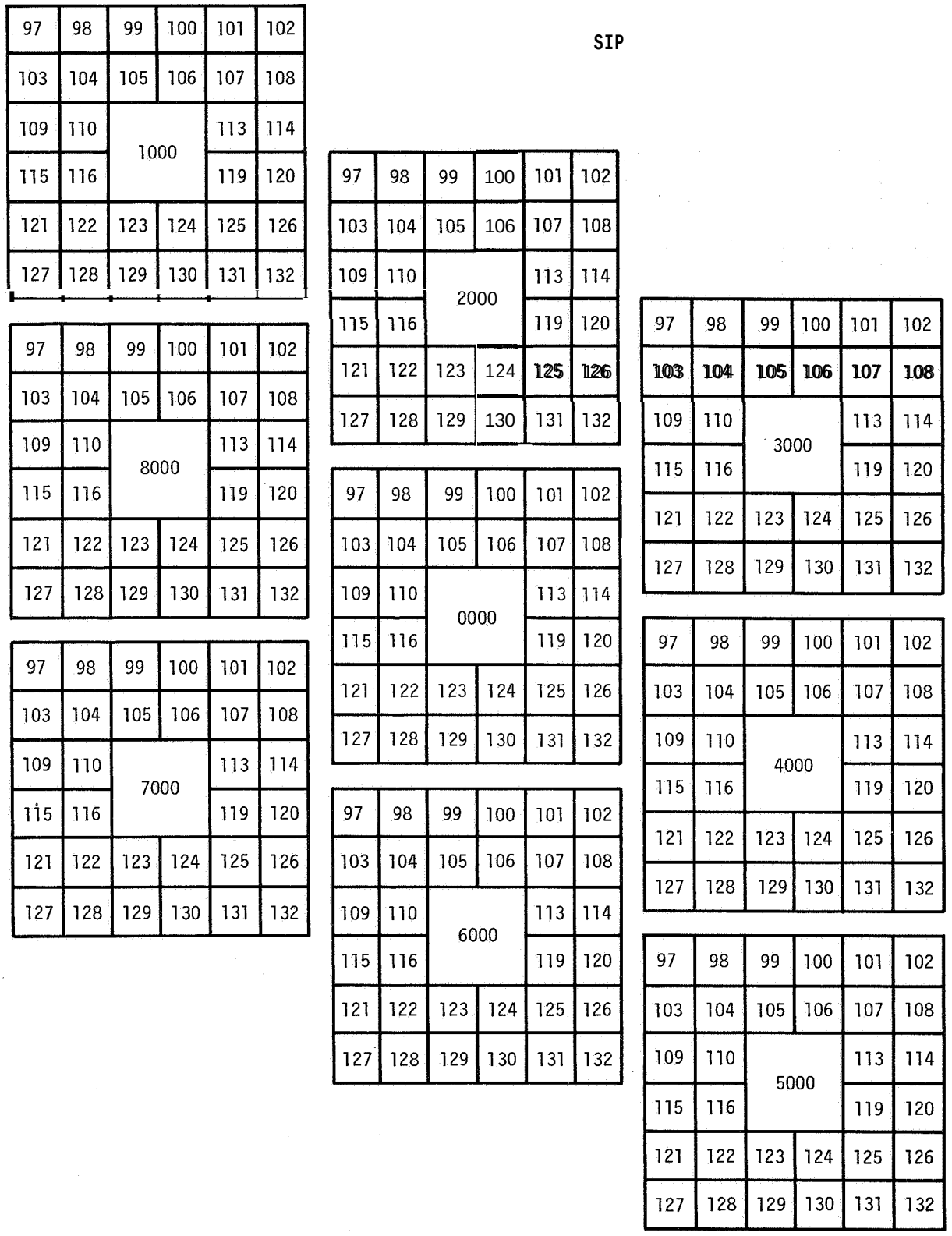

Figure 8.– Tile array showing nodes in **SIP**.

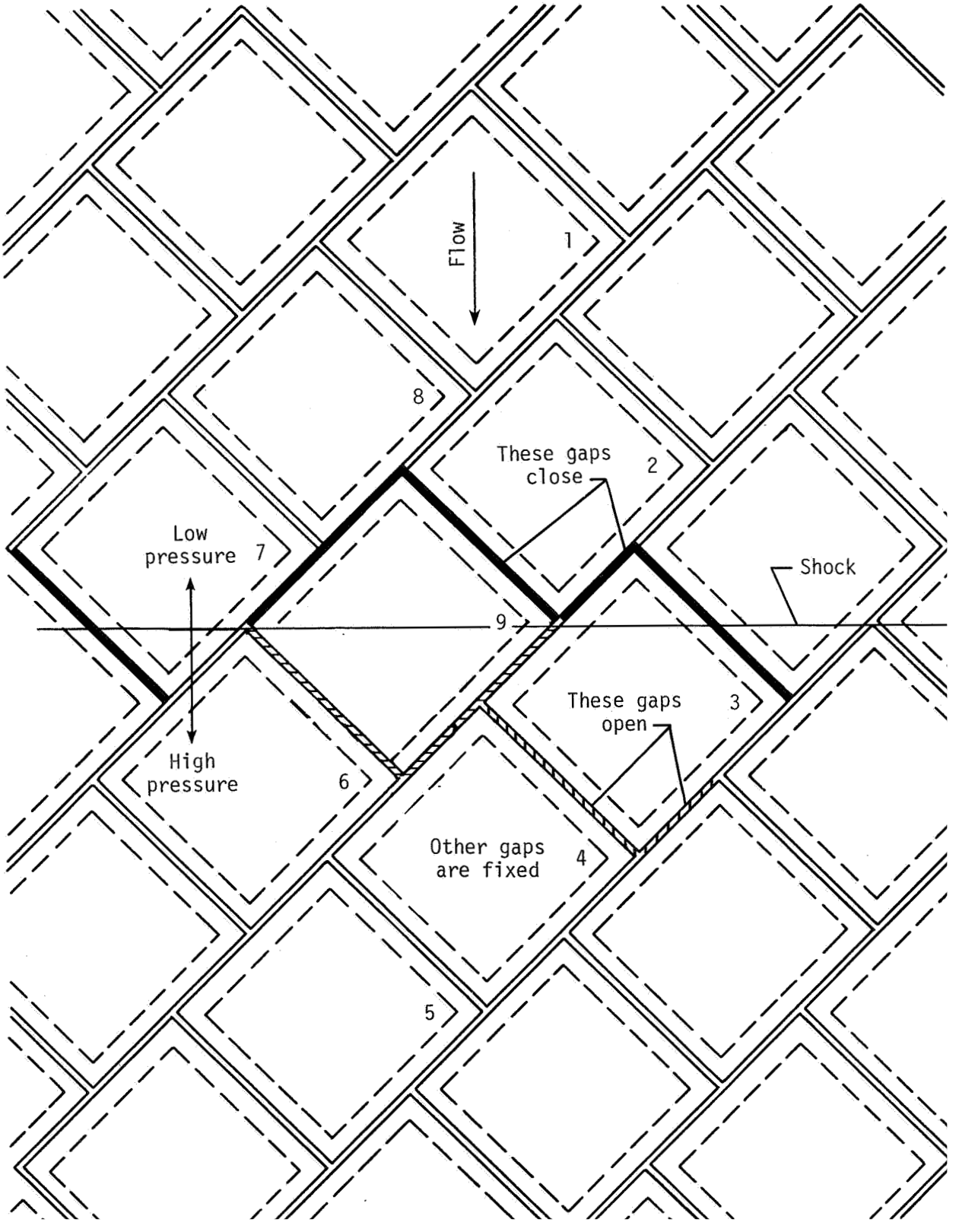

Figure 9.- Tile array showing gap changes due to x_1- and y_1-deflections.

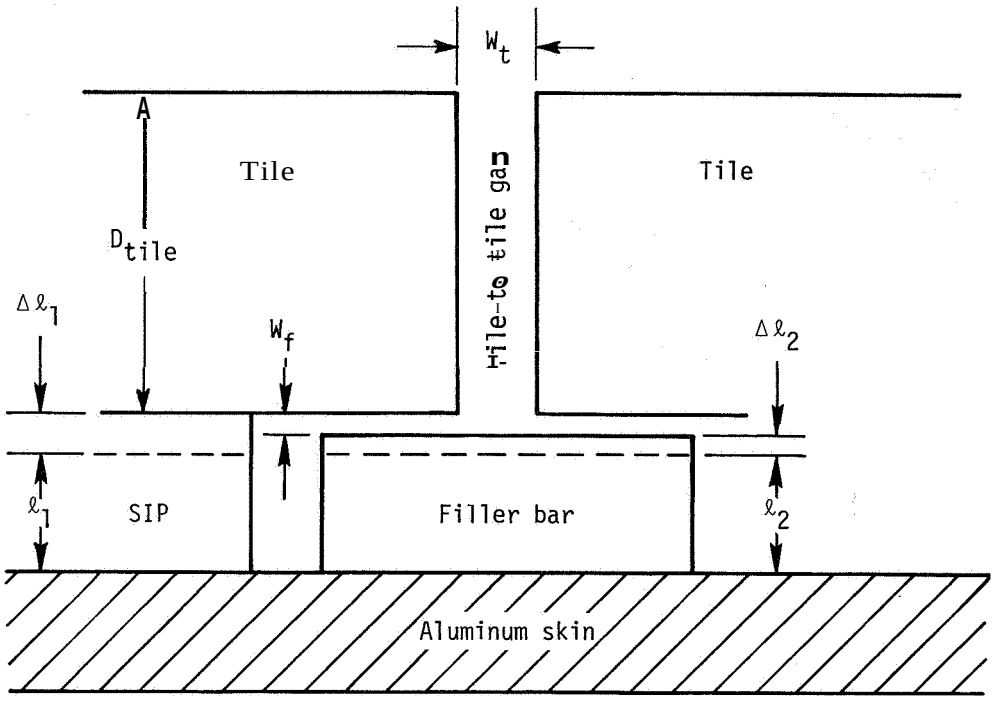

Figure 10.– **TPS** vertical dimensions and deflections caused by pressure loads.

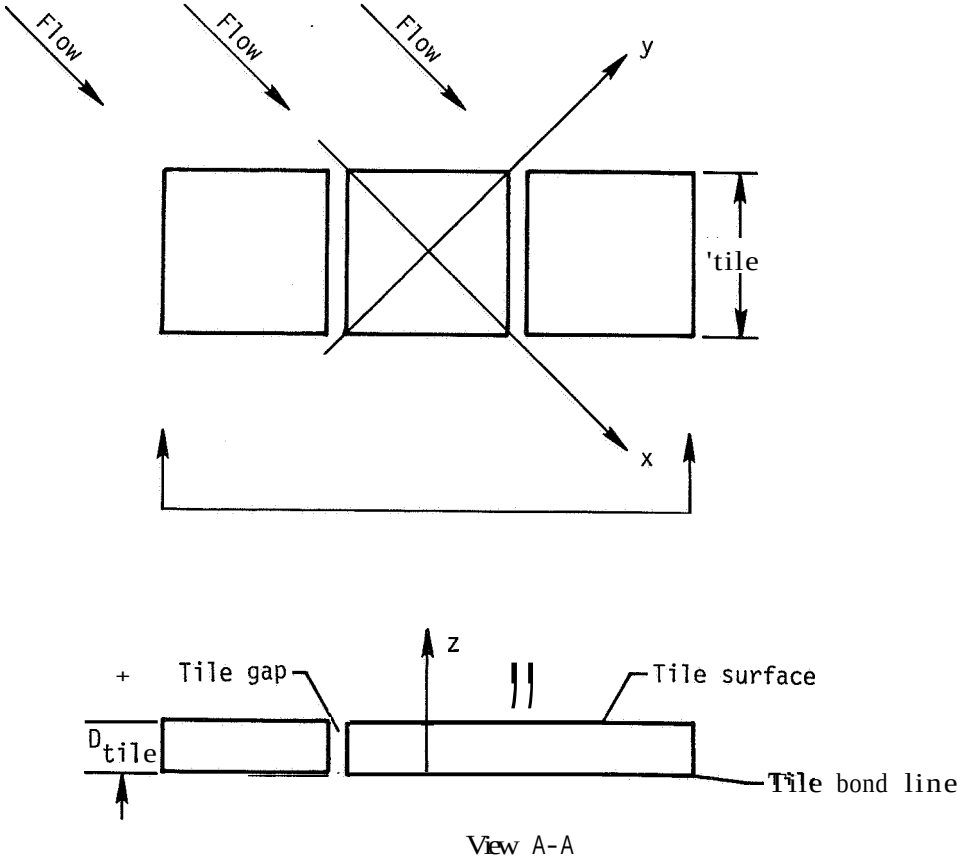

Figure 11.– Tile coordinate system for forces and moments.

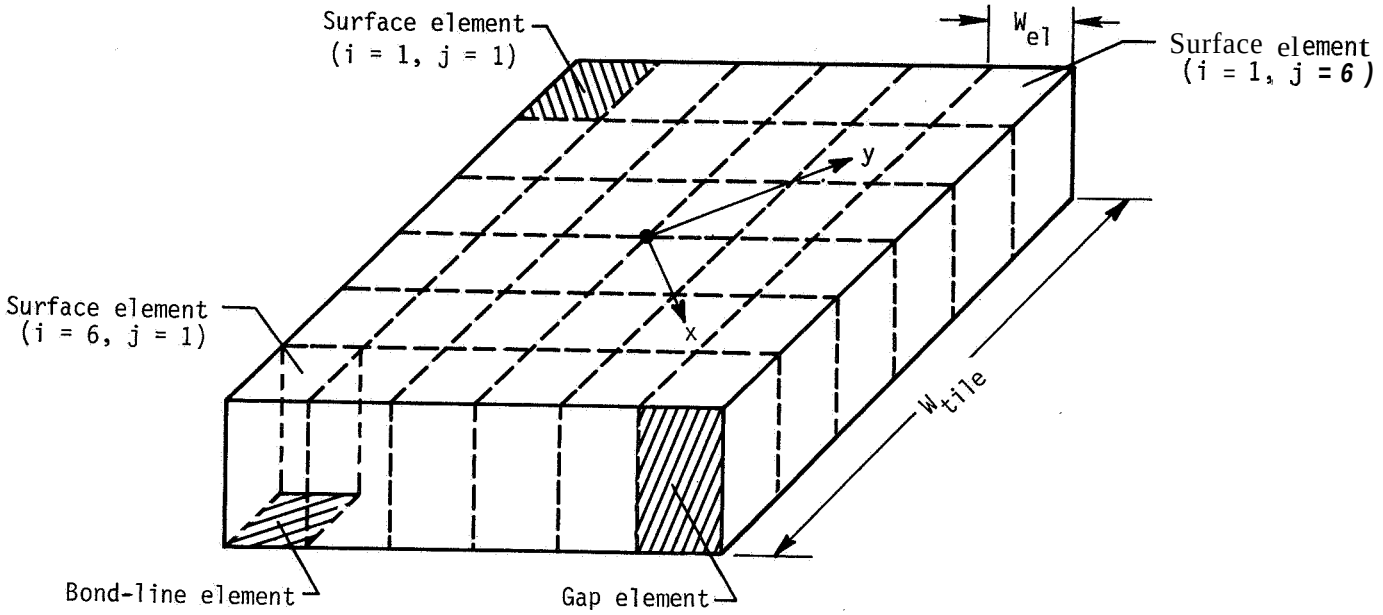

Figure 12.- Subject tile matrix formation. W_{tile} = 6 in.; W_{el} = 1 in.

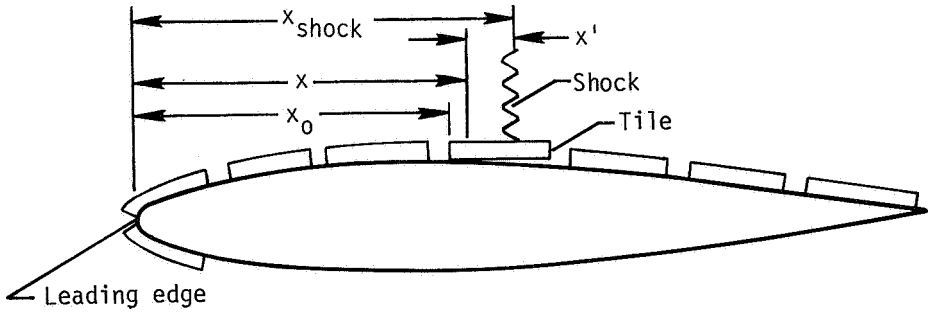

Figure 13.- Location of tile and shock from leading edge for calculation of skin friction.

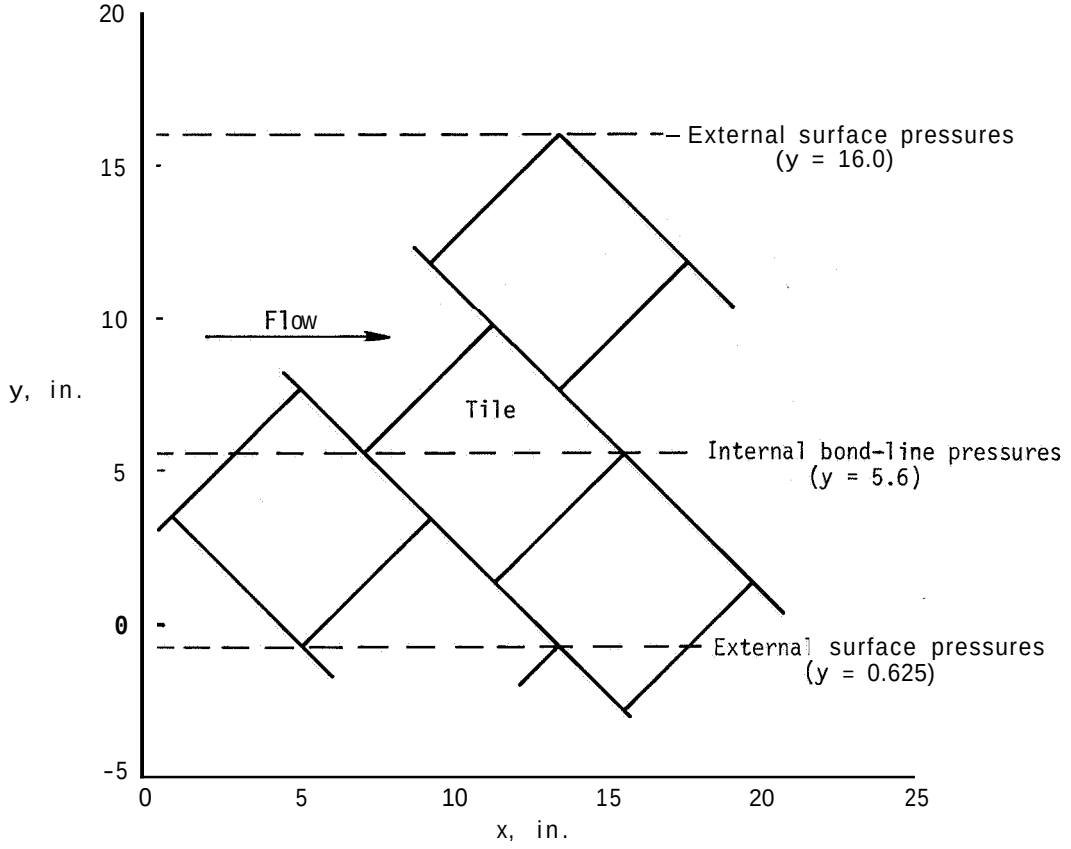

Figure 14.– Location of pressure measurements for OS36 wind–tunnel test with tiles mounted on SIP.

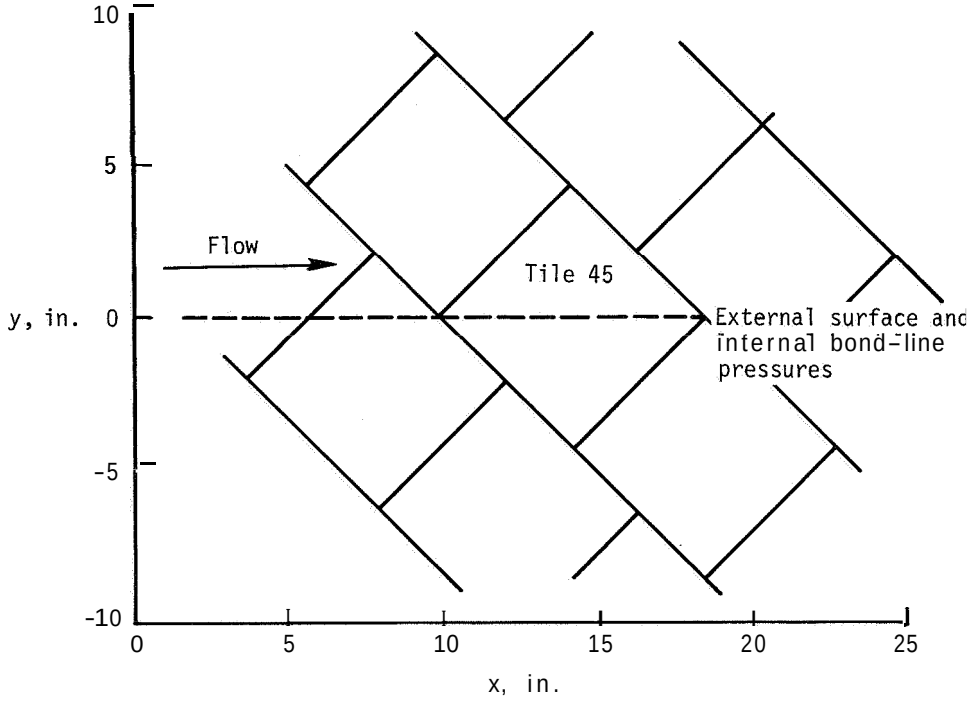

Figure 15.– Location of pressure measurements for OS55 wind–tunnel test with tiles mounted on SIP.

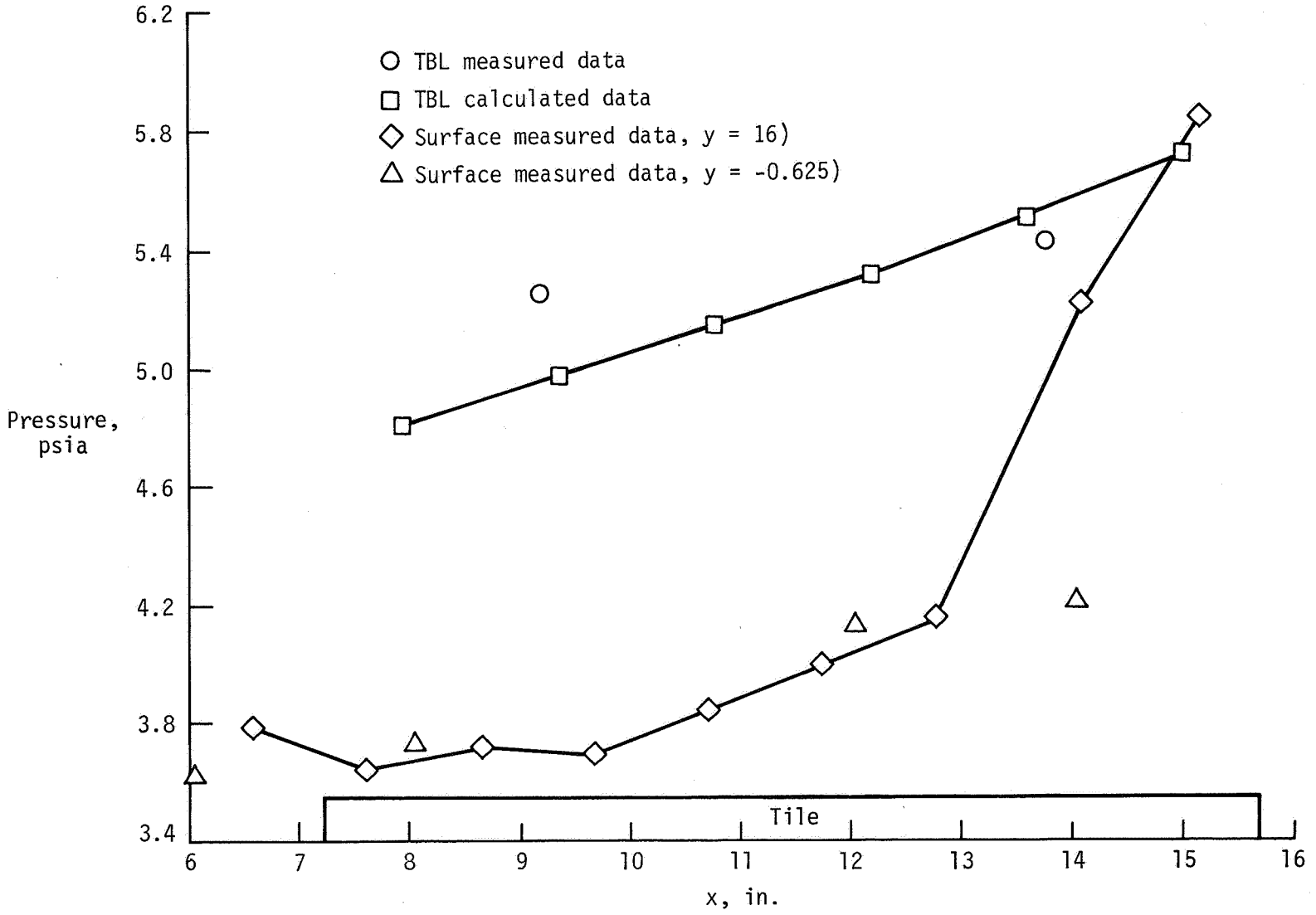

Figure 16.- Comparison of calculated and measured pressures at tile bond line for OS36 wind-tunnel test, run 202. LI900 undensified tile; M = 0.88; dynamic pressure, 647.5 psf; p = 1149 psf.

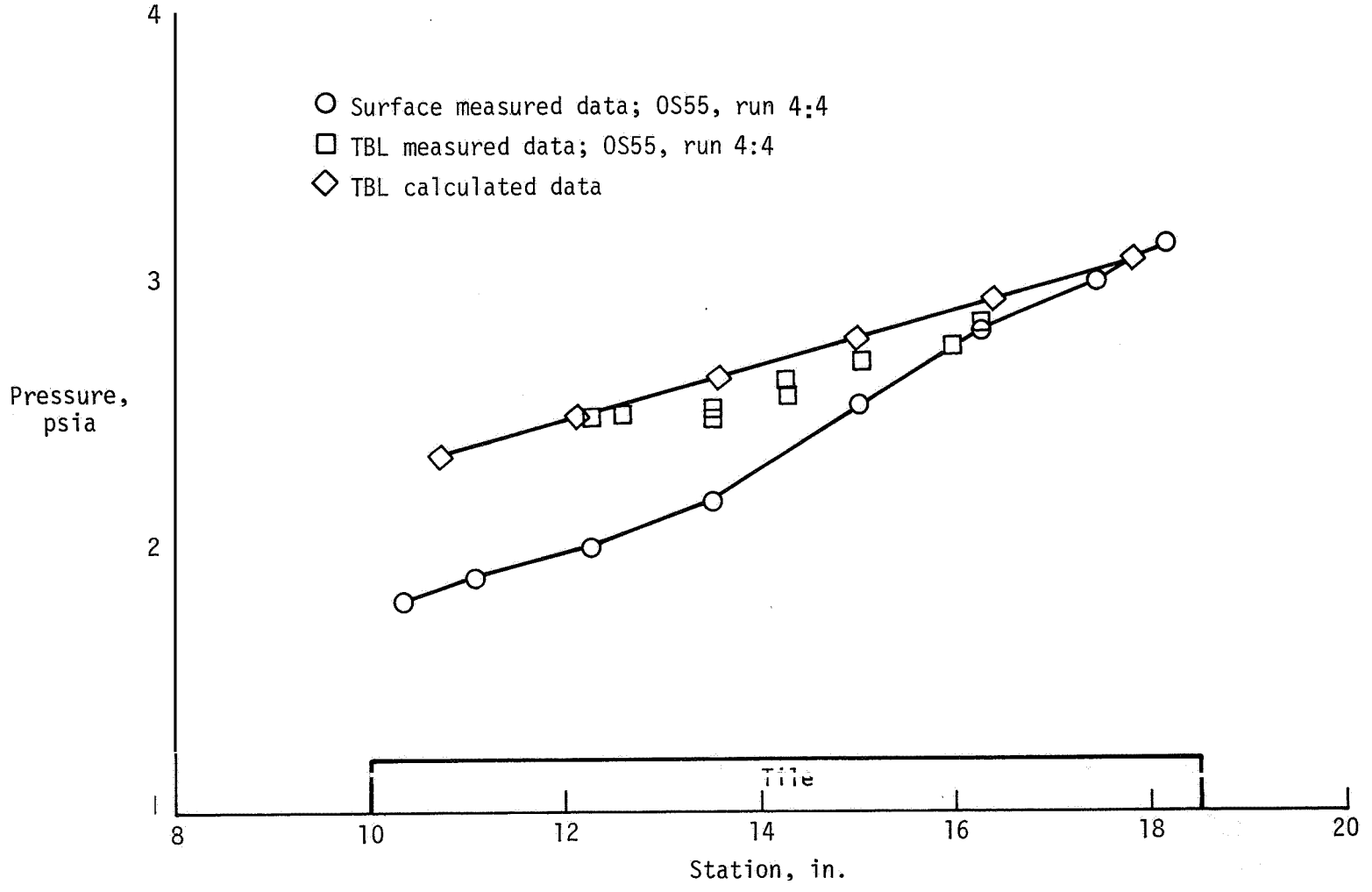

Figure 17.- Comparison of measured and calculated pressures at tile bond line for 5% wind-tunnel test, run 4:4. LI900 undensified tile.

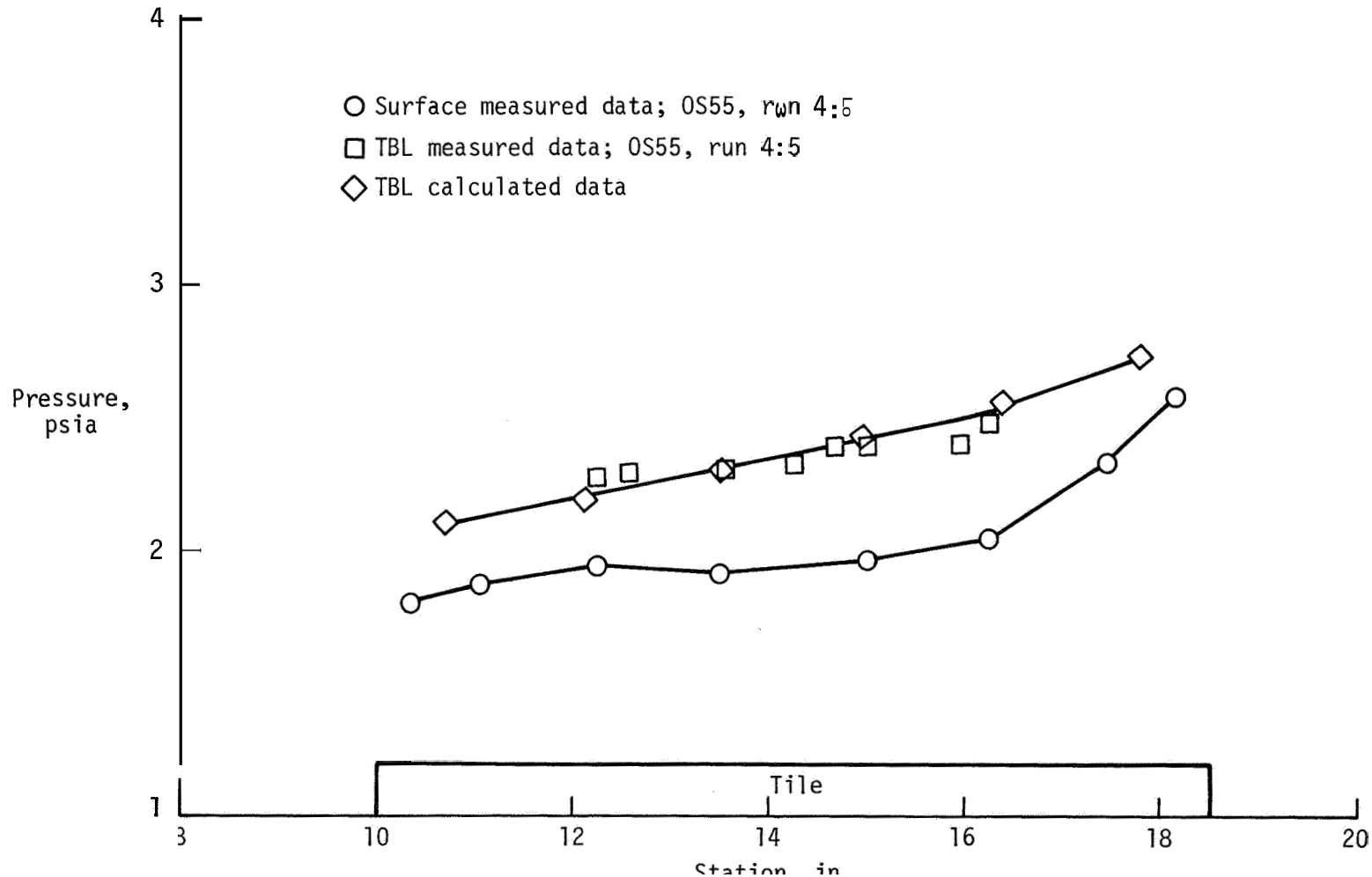

Figure 18.- Comparison of measured and calculated pressures at tile bond line for OS55 wind-tunnel test, run 4:5. LI900 undensified tile.

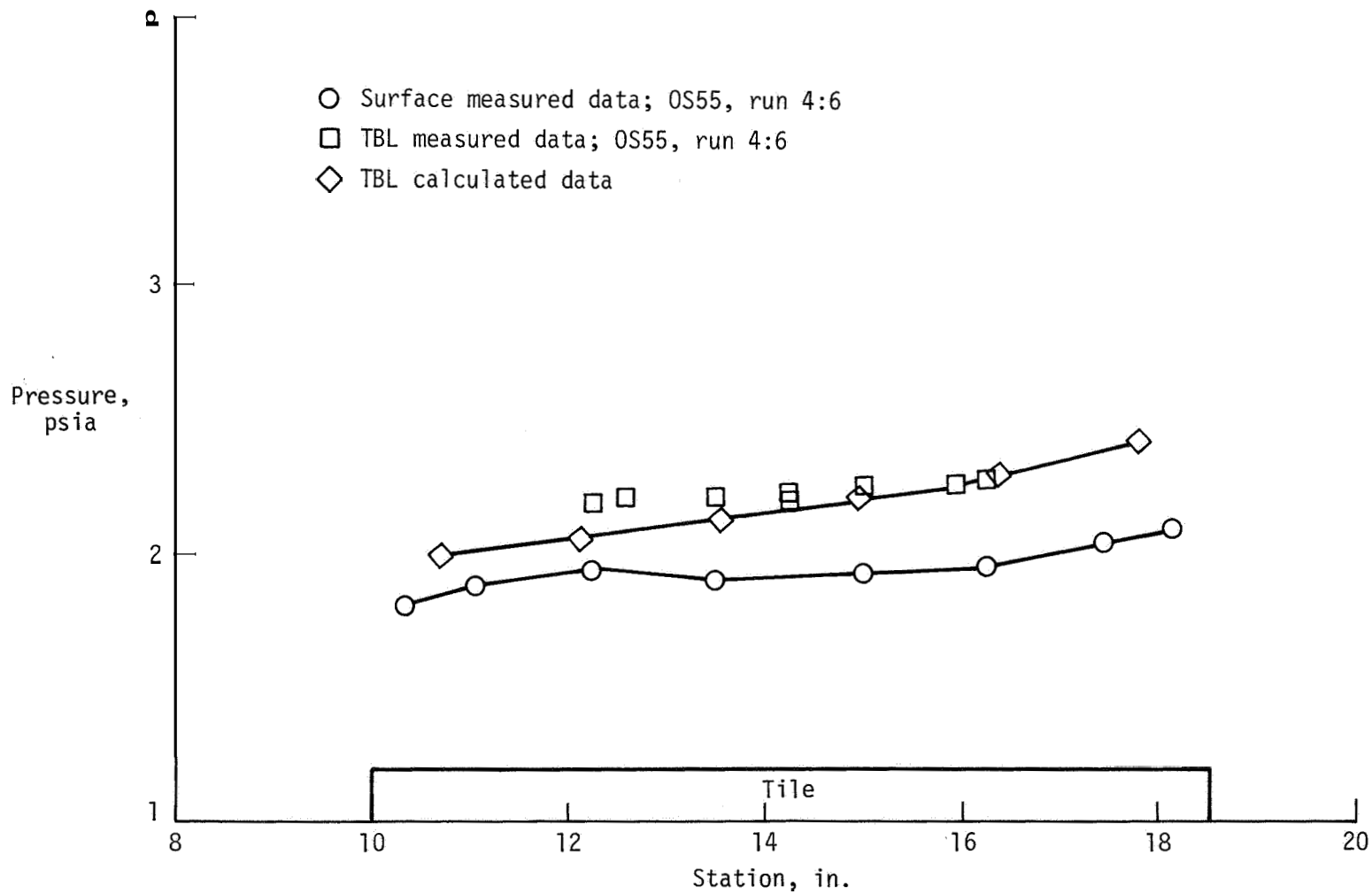

Figure 19.- Comparison of measured and calculated pressures at tile bond line for OS55 wind-tunnel test, run 4:6. LI900 undensified tile.

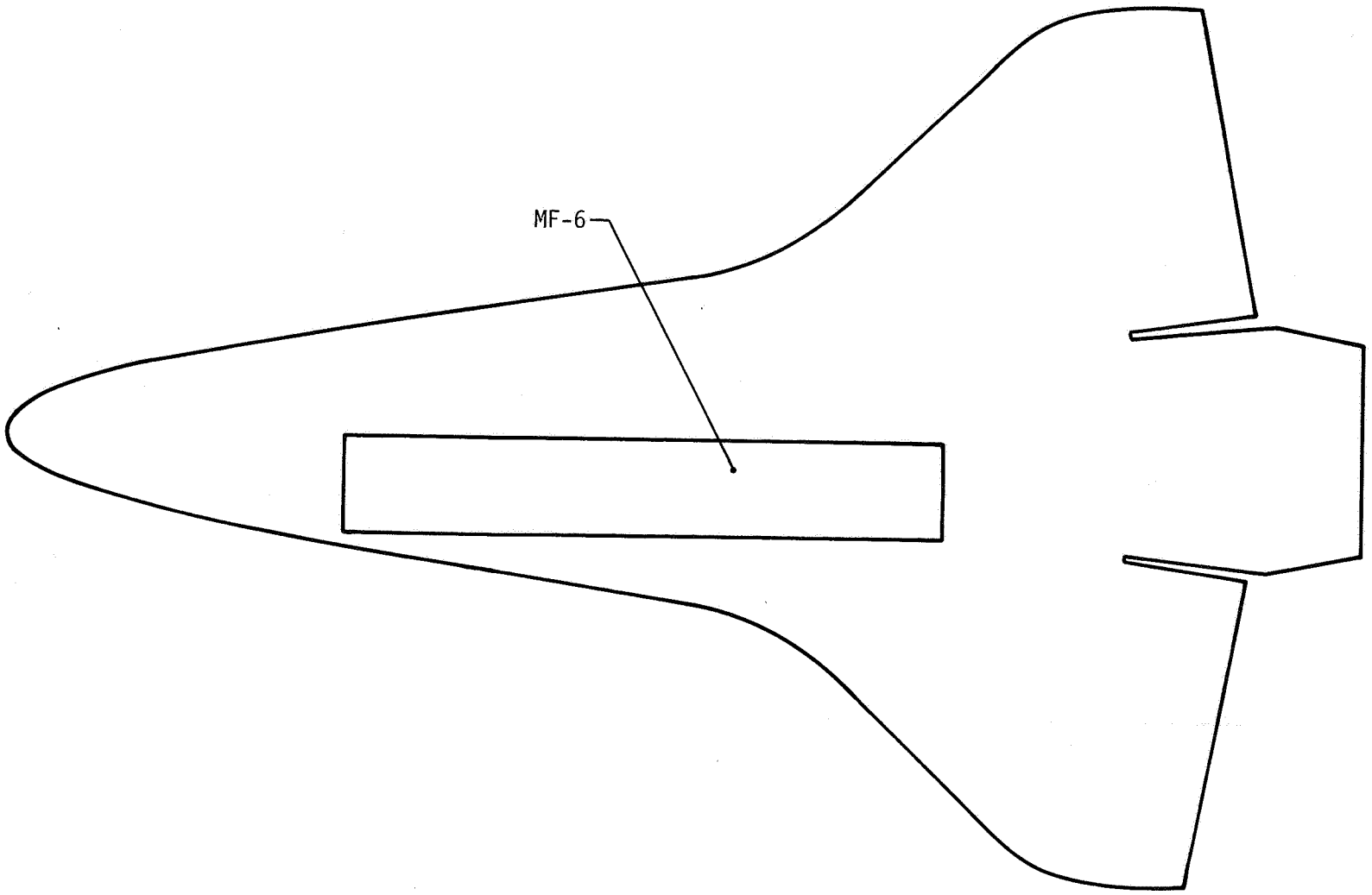

Figure 20.— Mid-fuselage, zone 6 (MF-6) region on lower surface of orbiter.

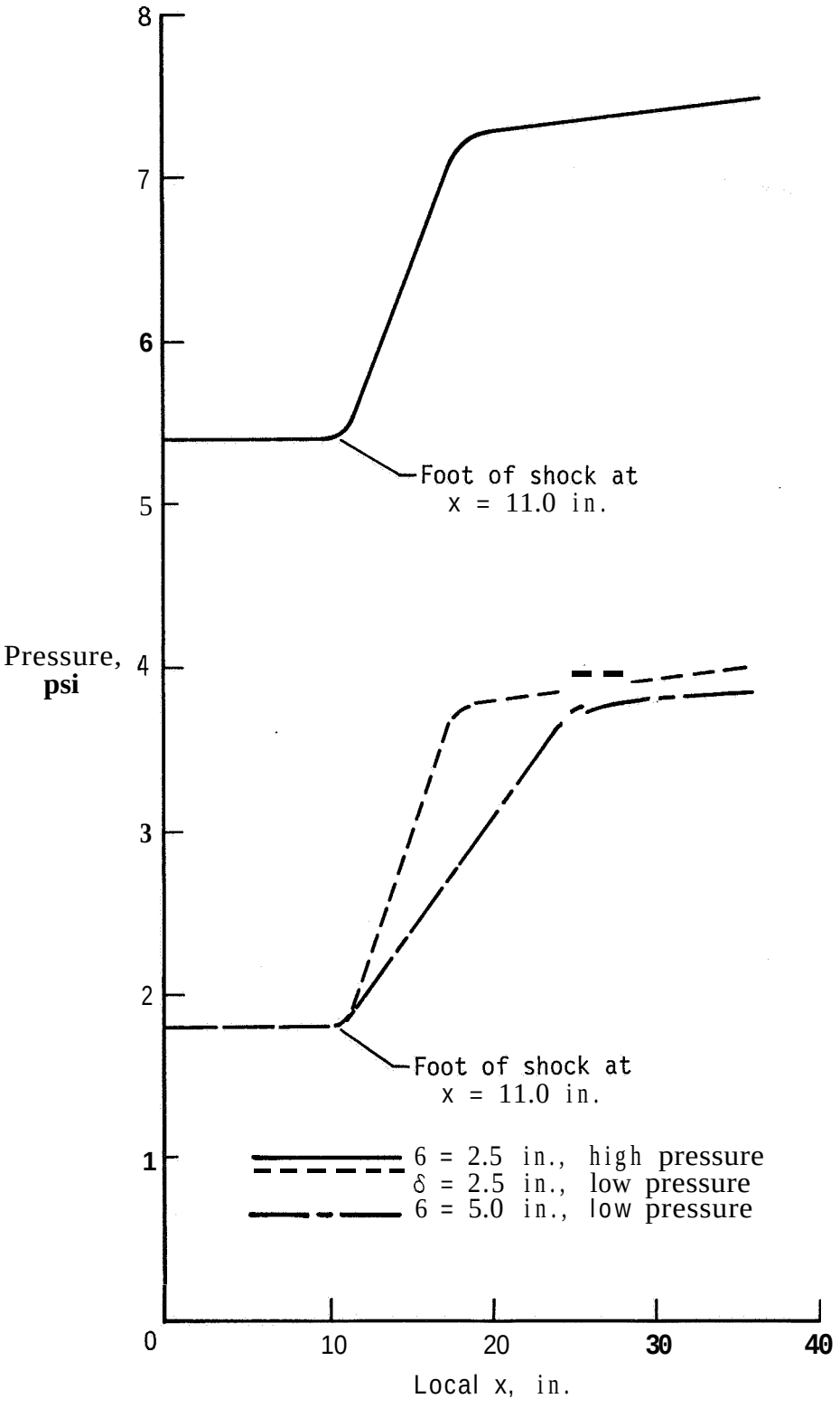

Figure 21.– MF-6 pressure profiles.

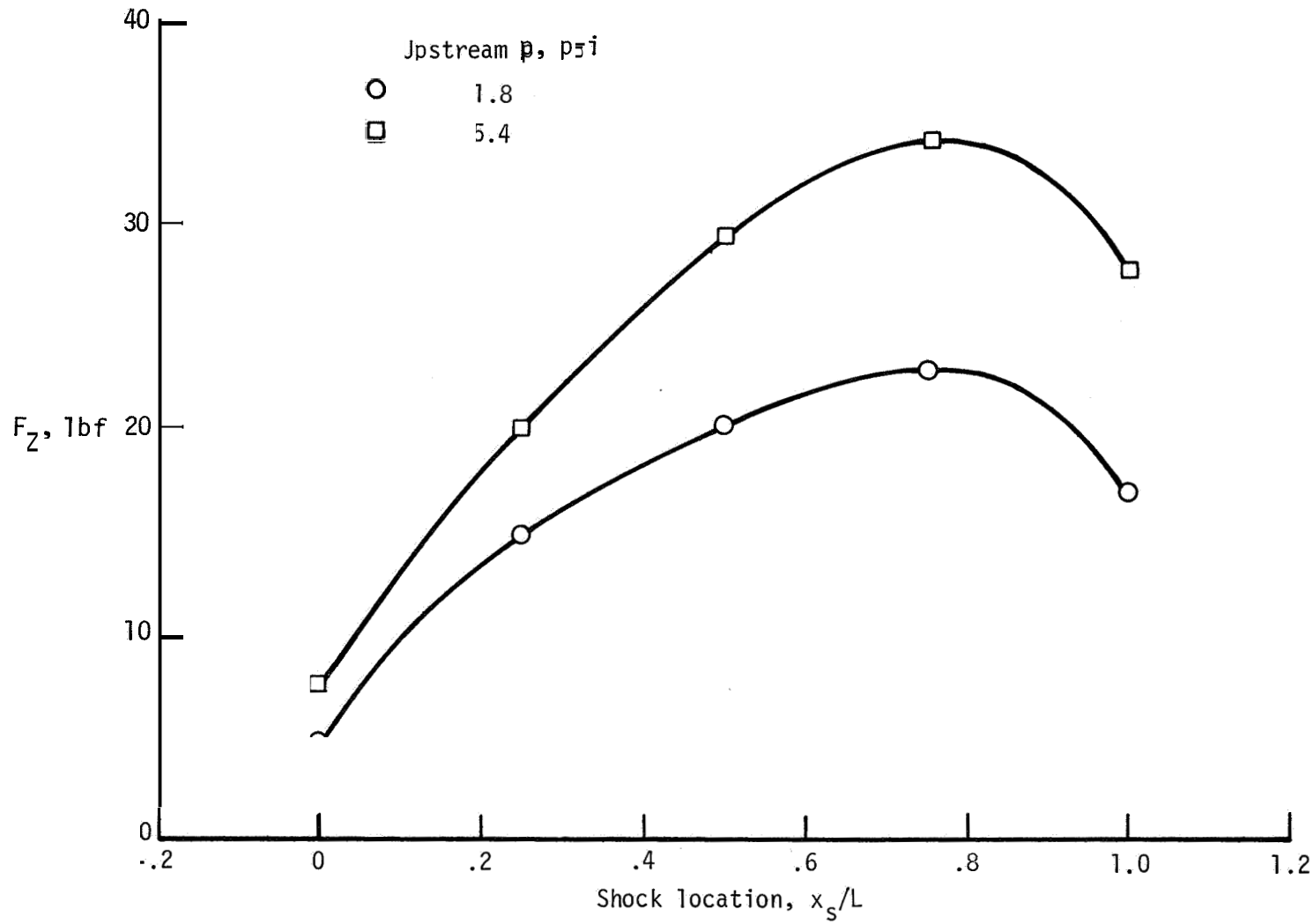

(a) Normal force; 2-psi shock; 2.5-in-thick boundary layer; 1-in-thick tile.

Figure 22.- Calculated normal force and moment as function of shock location in MF-6 region for LI900 undensified tile.

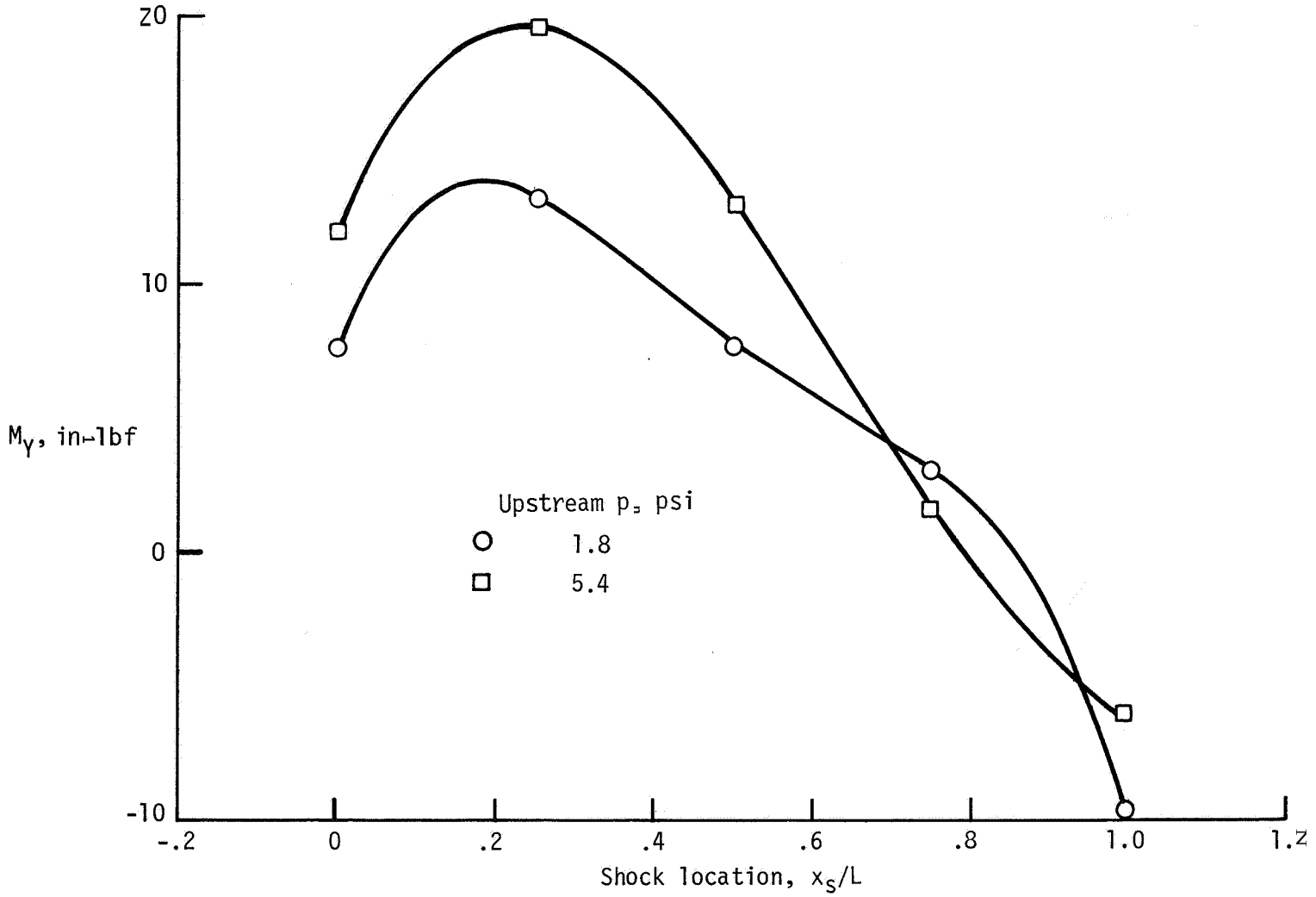

(b) Moment; 2-psi shock; 2.5-in-thick boundary layer; 1-in-thick tile.

Figure 22.- Continued.

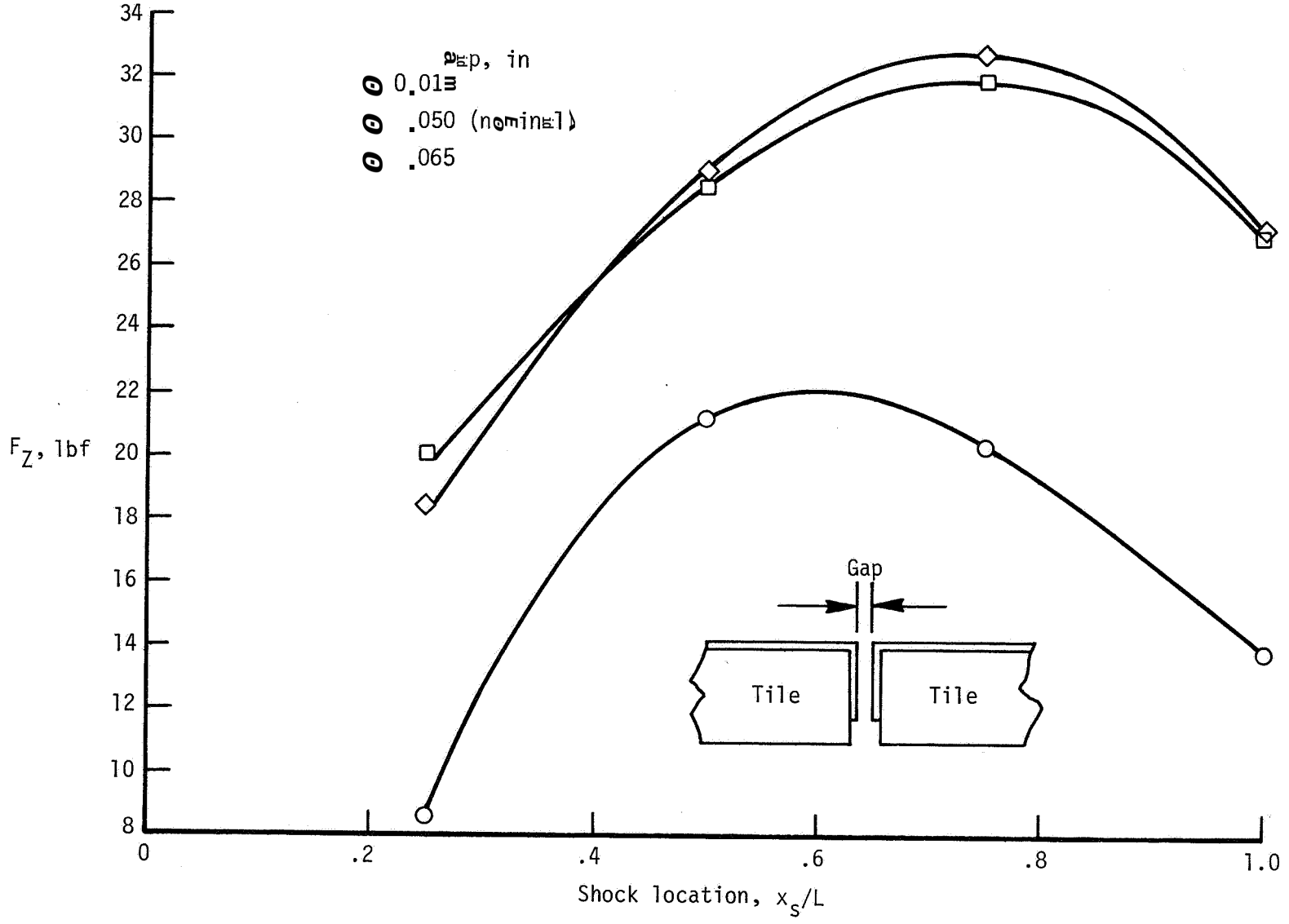

(c) Normal force; high-pressure shock; 2.5-in-thick boundary layer; 2-in-thick tile.

Figure 22.- Continued.

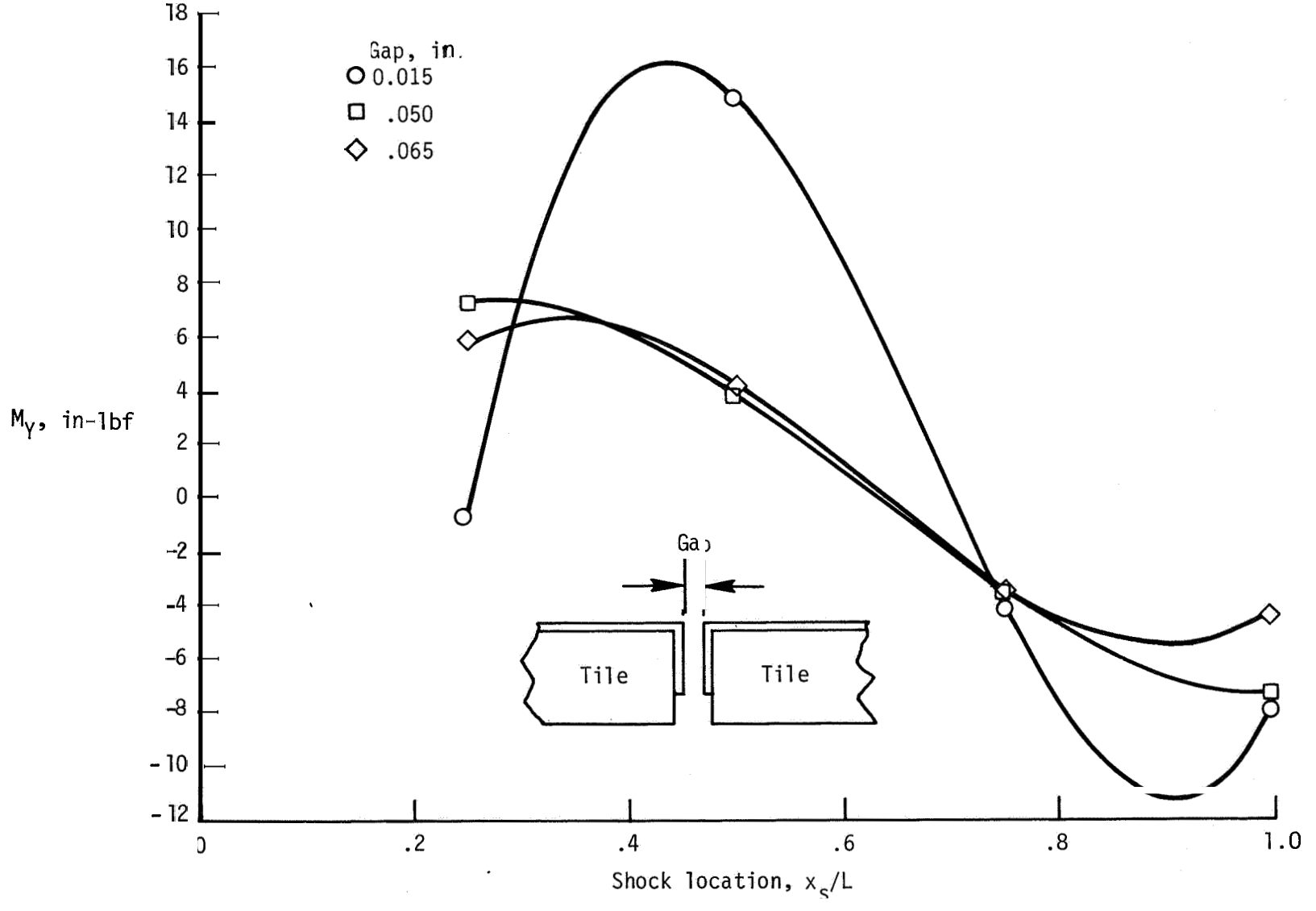

(d) Moment; high-pressure shock; 2.5-in-thick boundary layer; 2-in-thick tile.

Figure 22.- Continued.

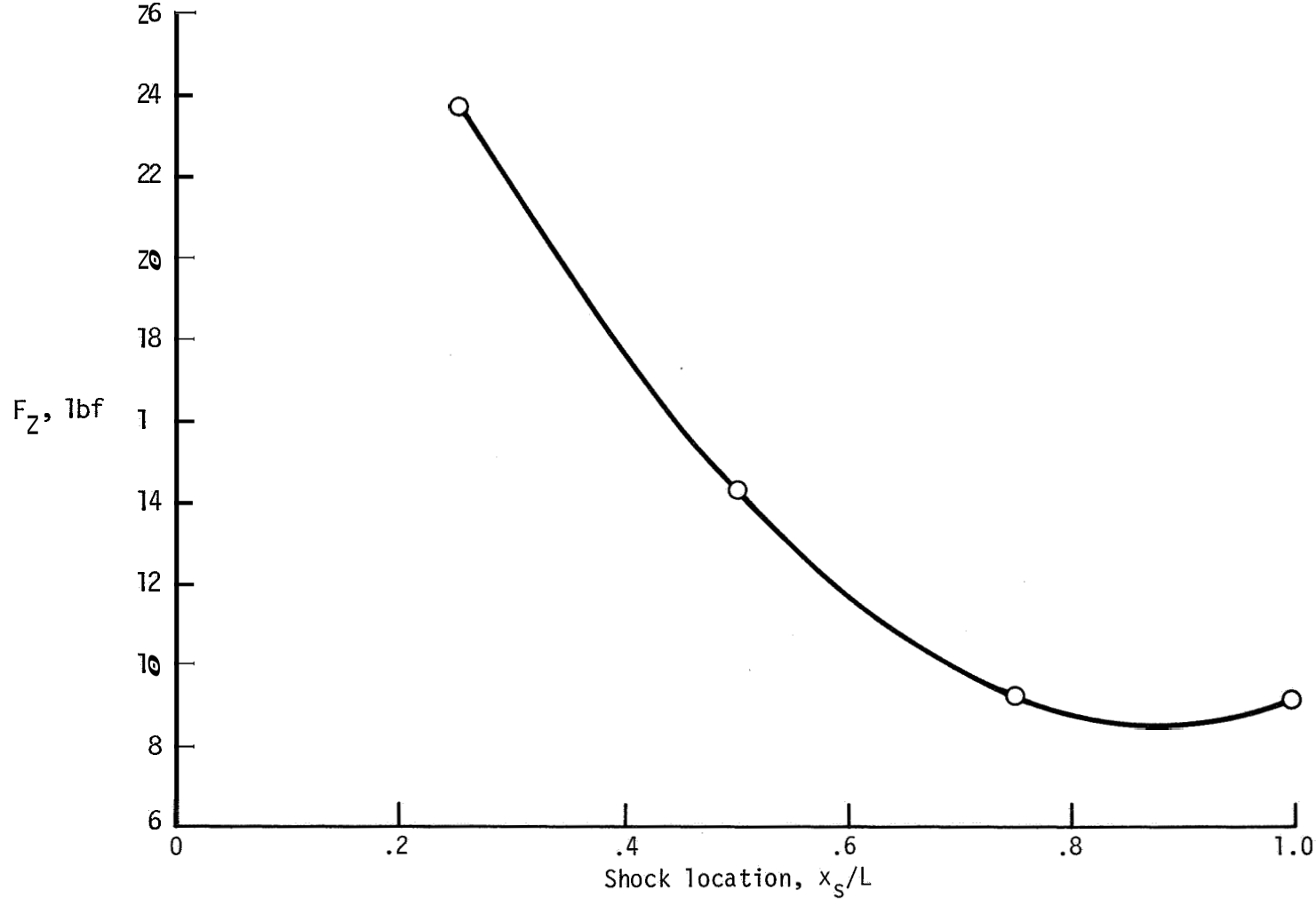

(e) Normal force; low-pressure shock; 5-in-thick boundary layer; 1-in-thick tile.

Figure 22.- Continued.

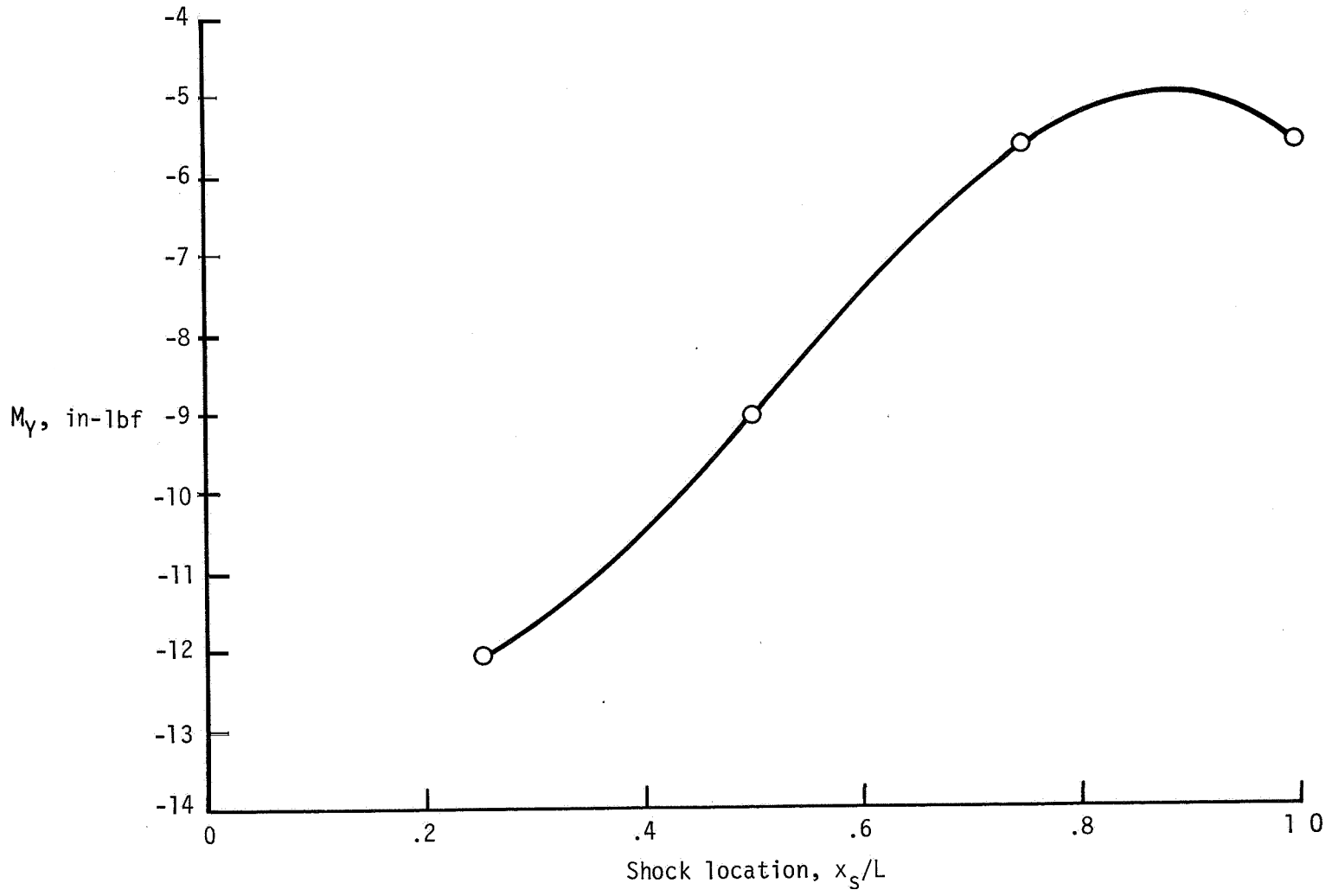

(f) Moment; low-pressure shock; 5-in-thick boundary layer; 1-in-thick tile.

Figure 22.- Concluded.

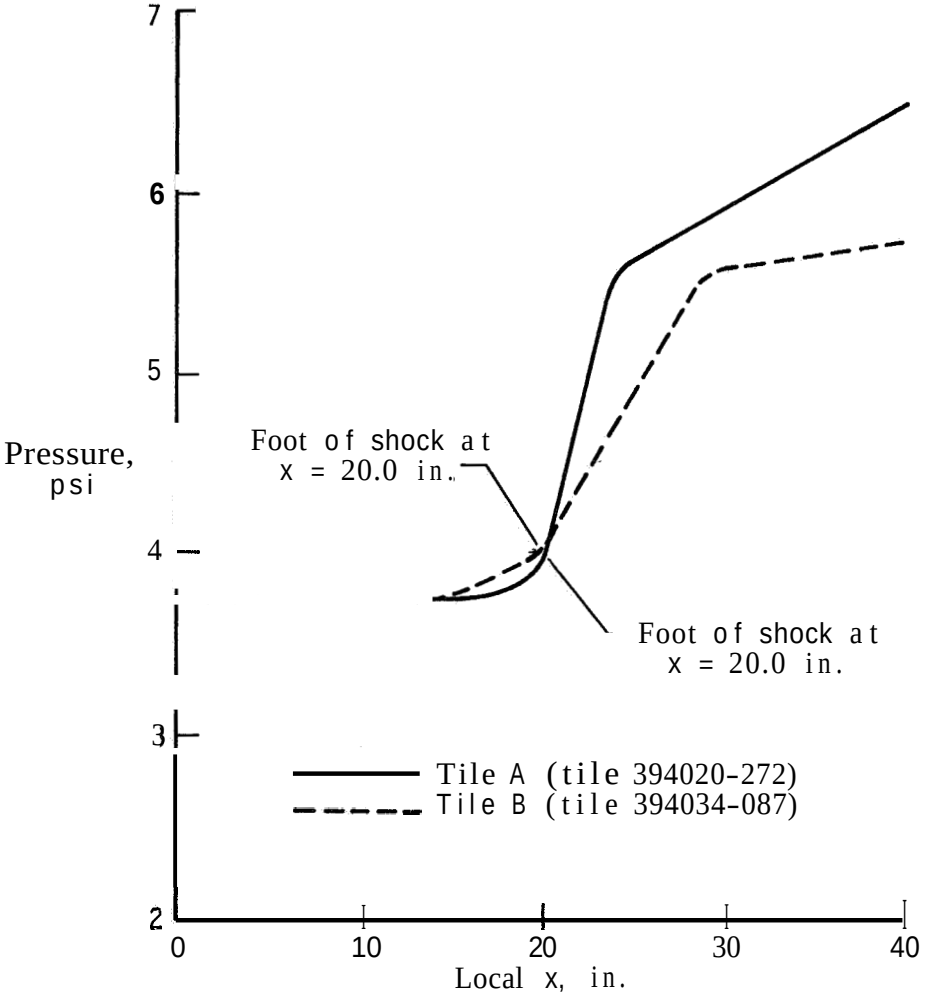

Figure 23.- MF-6 pressure profiles.

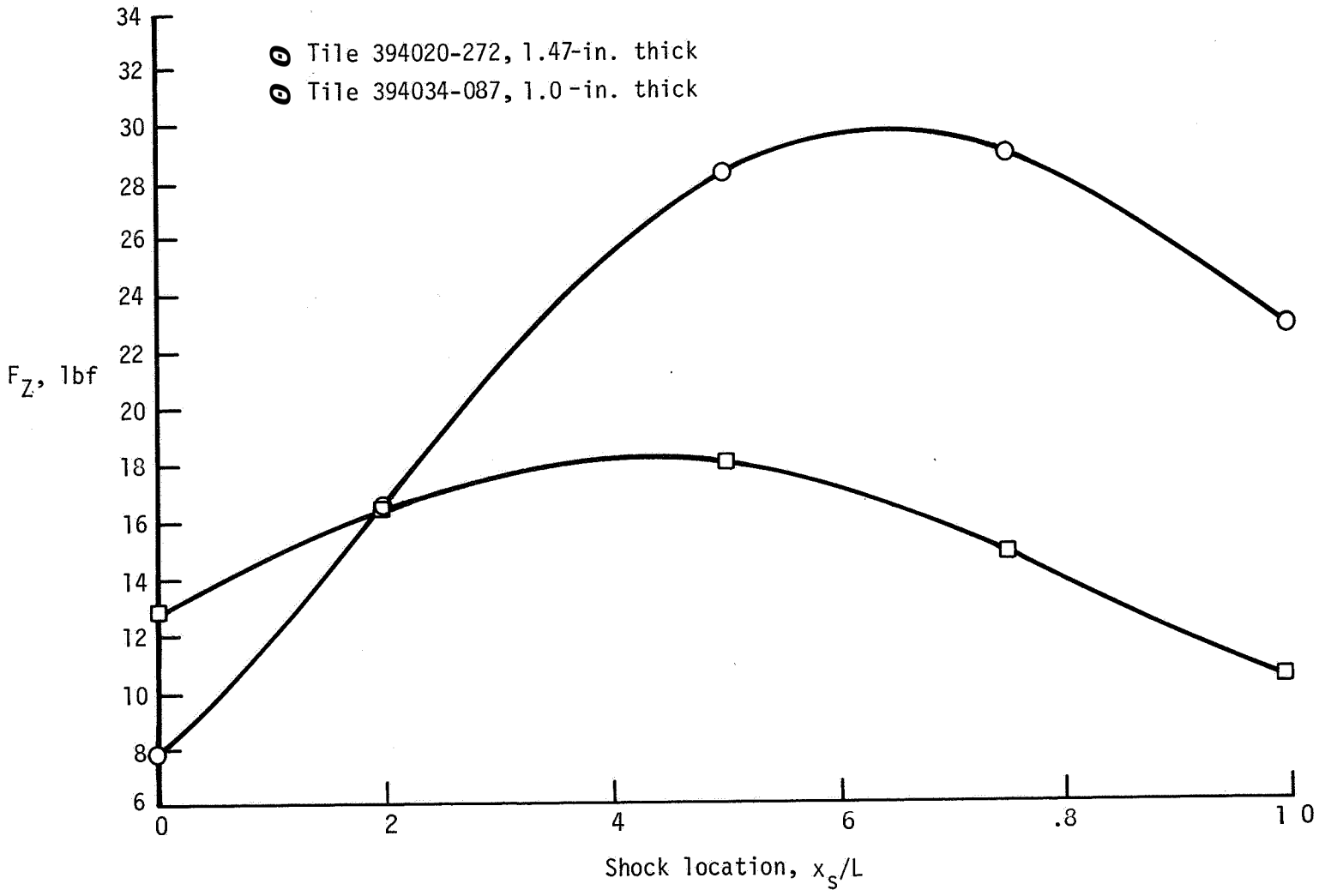

(a) Normal force; nominal tile gap, 0.05 in.

Figure 24.- Calculated normal force and moment as function of shock location in MF-6 region for LI900 undensified tile with separated shocks.

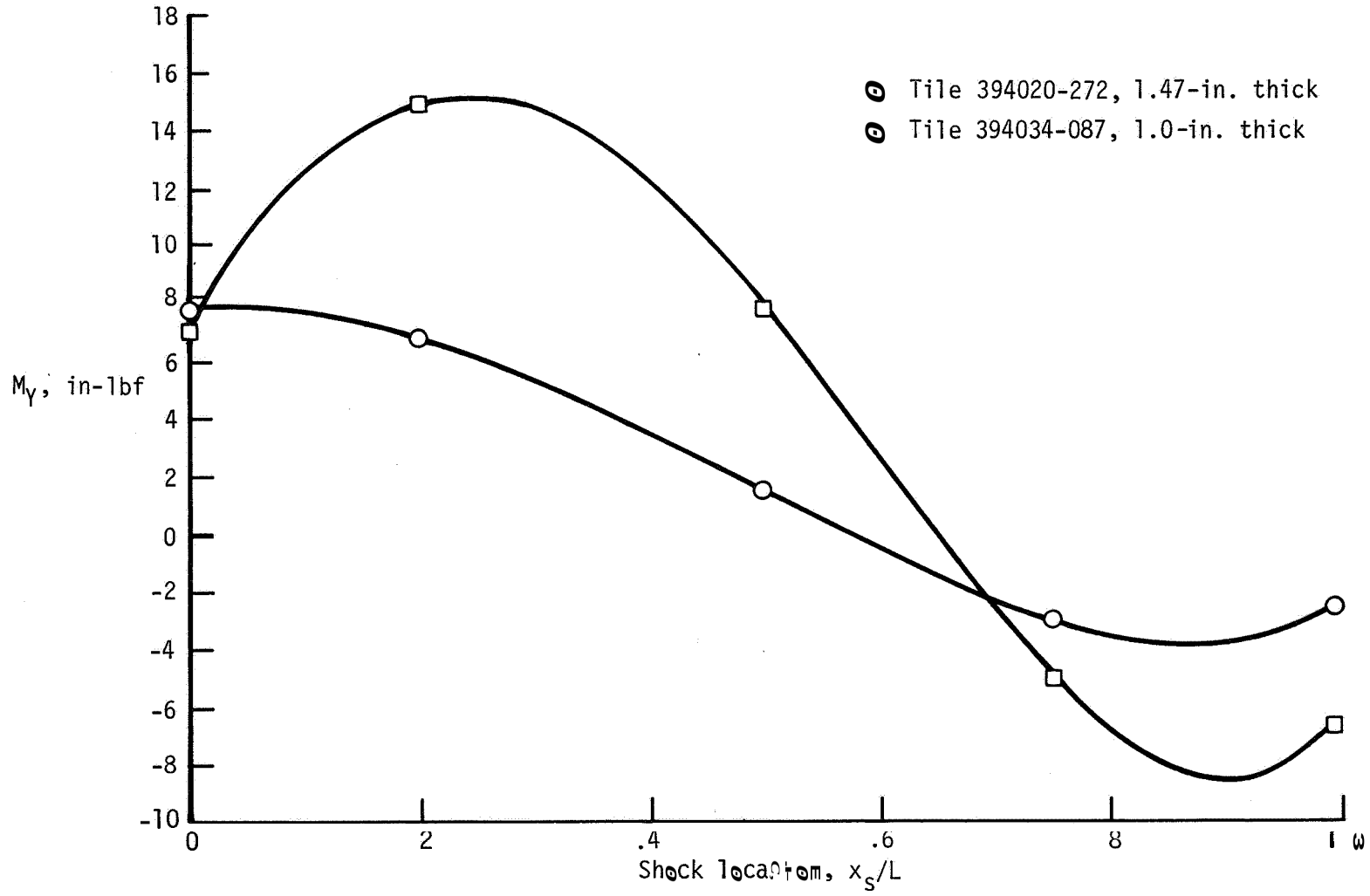

(b) Moment; nominal tile gap, 0.05 in.

Figure 24.- Concluded.

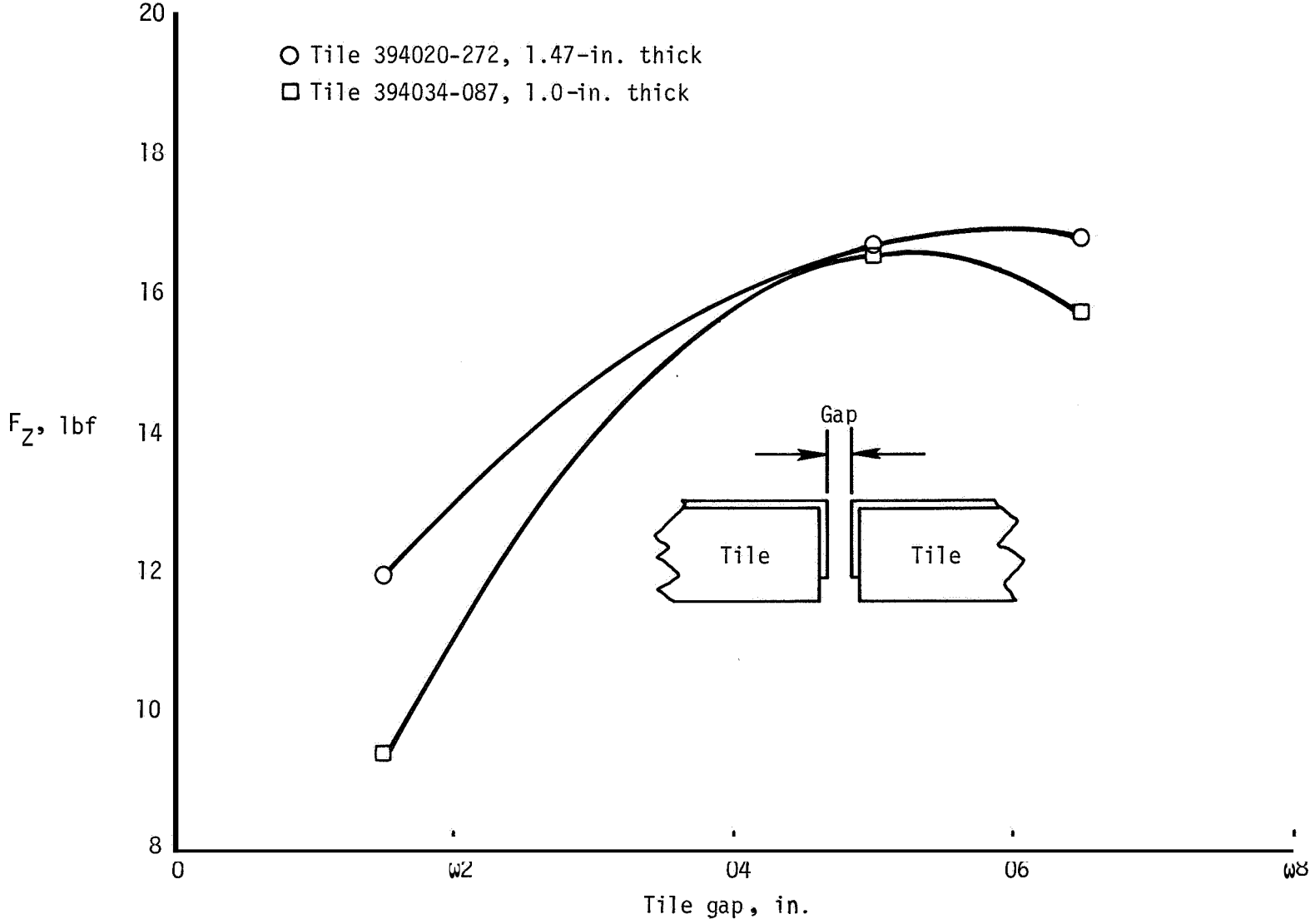

(a) Normal force; shock location at $x_s = 0.2L$.

Figure 25.- Calculated normal force and moment as function of tile gap in MF-6 region for LI900 undensified tile with separated shocks.

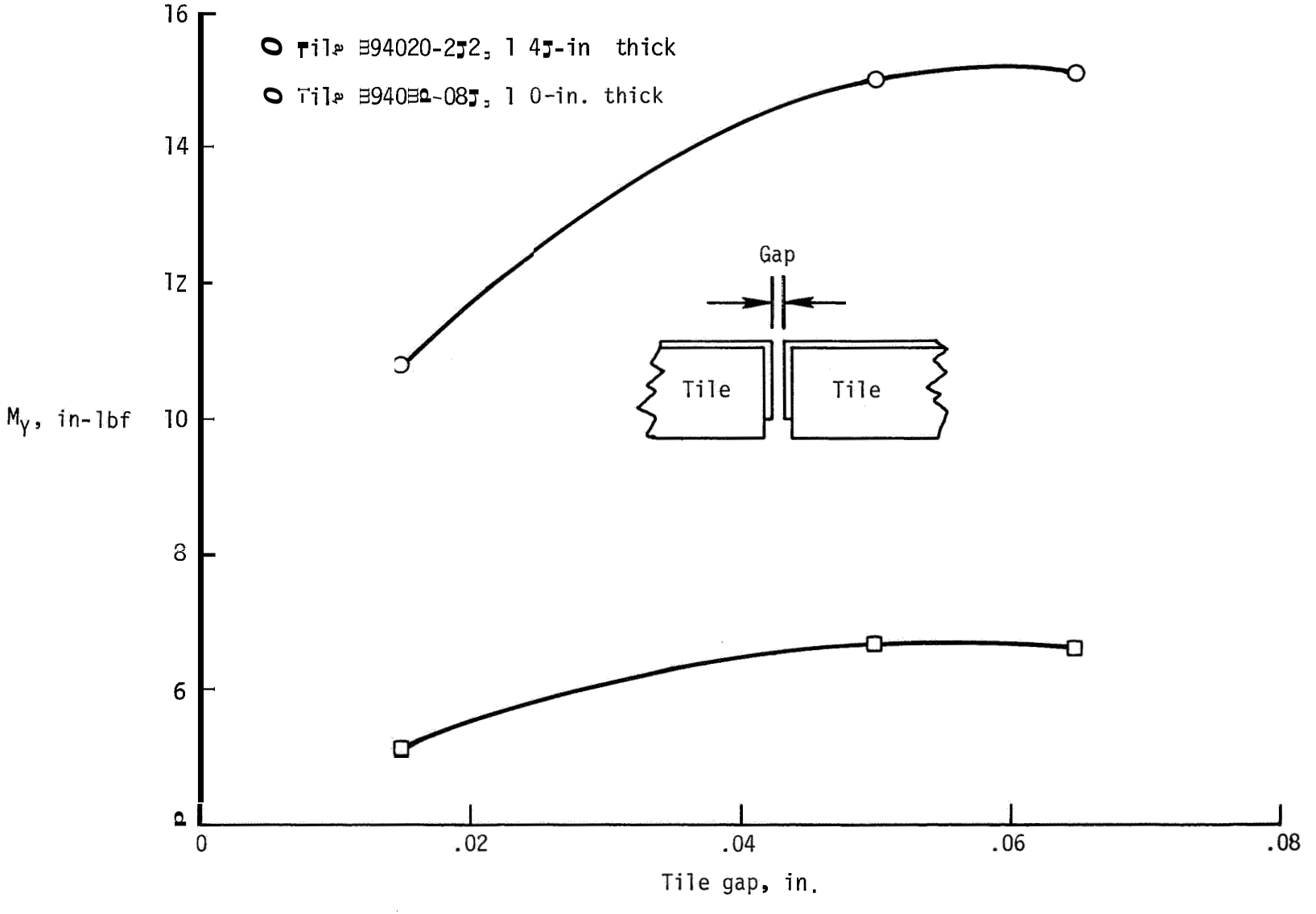

(b) Moment; shock location at $x_s = 0.2L$.

Figure 25.- Concluded.

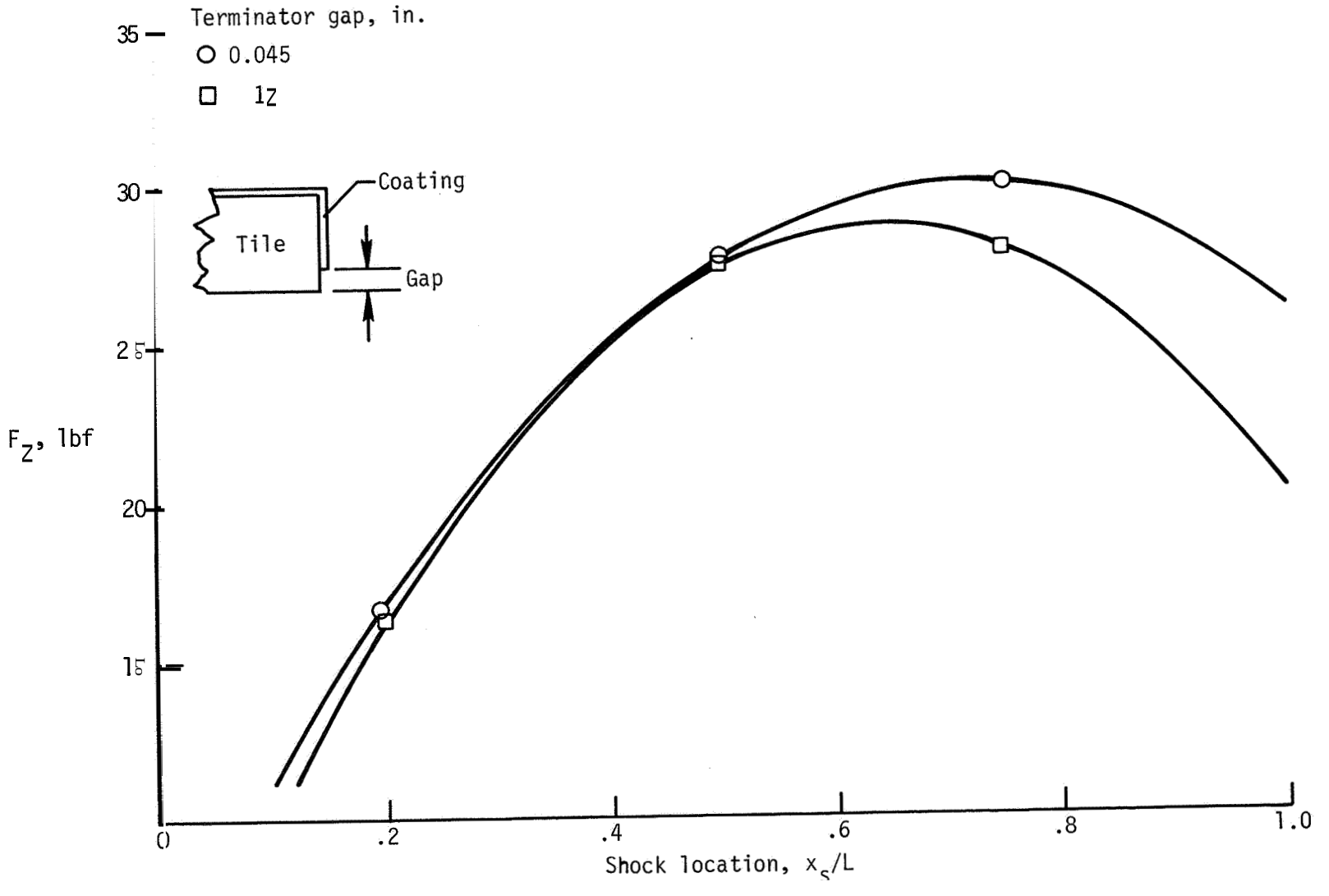

(a) Normal force; terminator gap; nominal terminator gap, 0.05 in.

Figure 26.- Calculated normal force and moment as function of shock location for MF-6 region, pressure profile A, separated shock, LI900 undensified tile 394020-272, and tile thickness of 1.47 in.

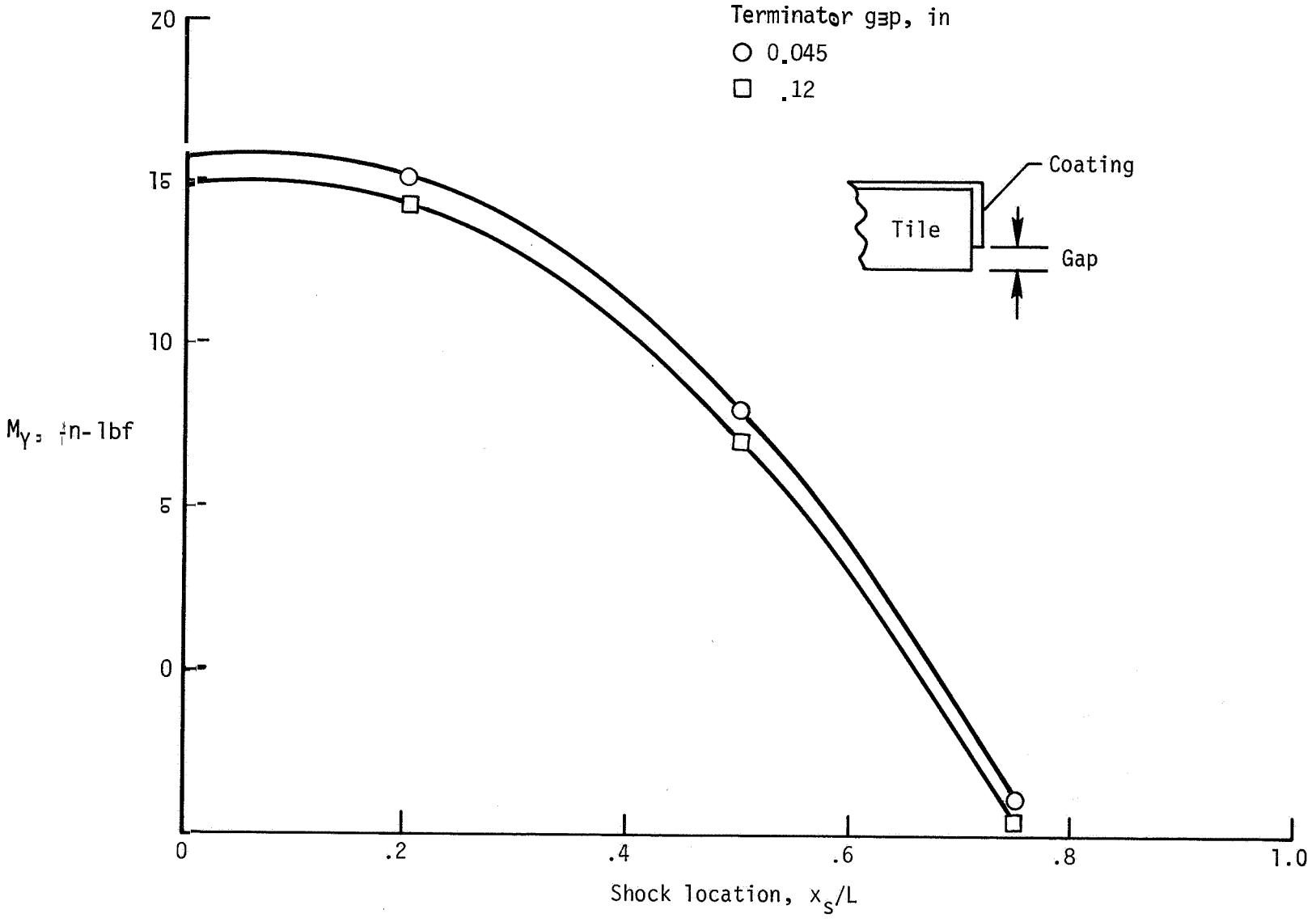

(b) Moment; terminator gap; nominal terminator gap, 0.0 in.

Figure 26.- Continued.

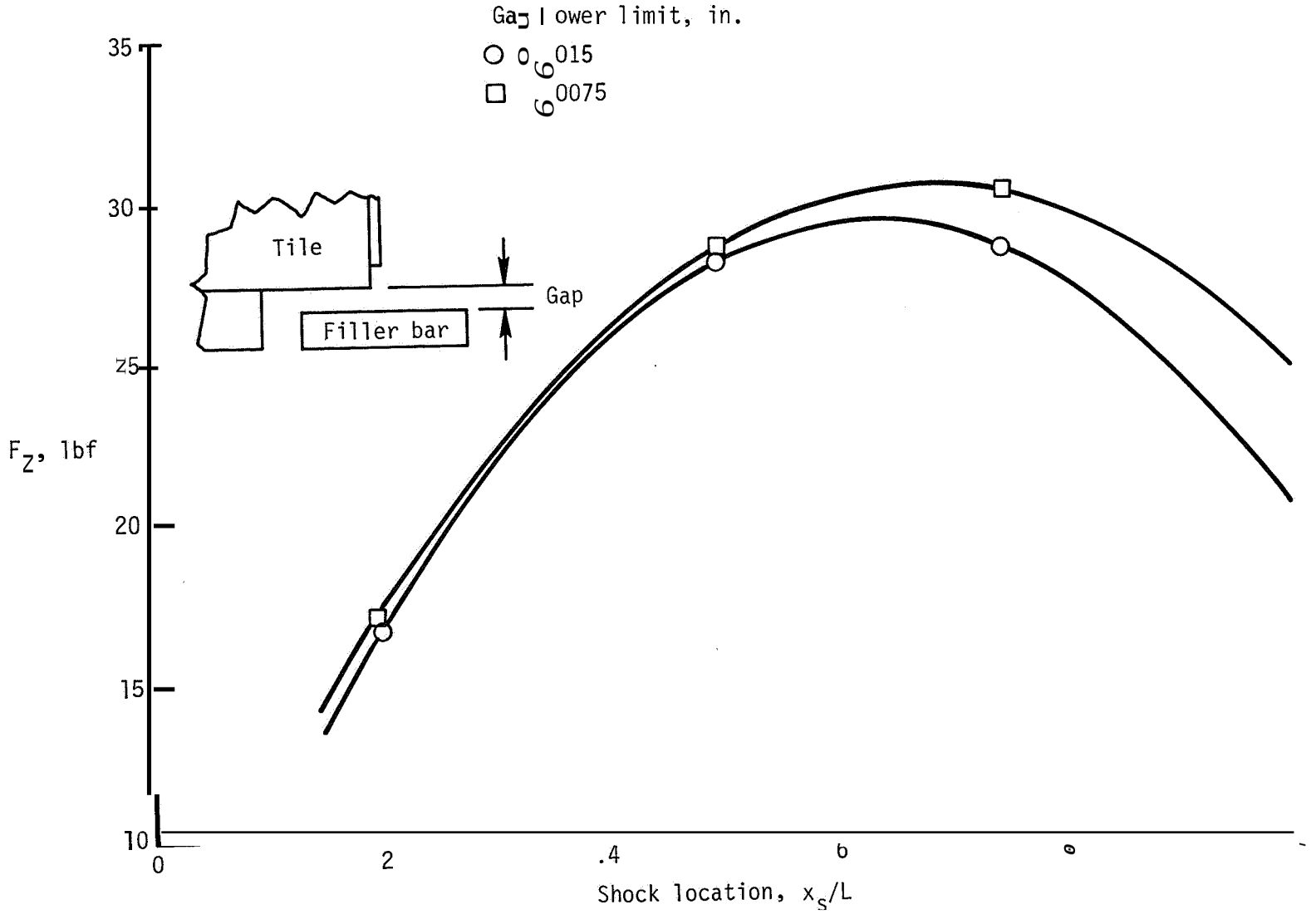

(c) Normal force; gap between filler bar and tile; nominal lower limit, 0.001 in.

Figure 26.- Continued.

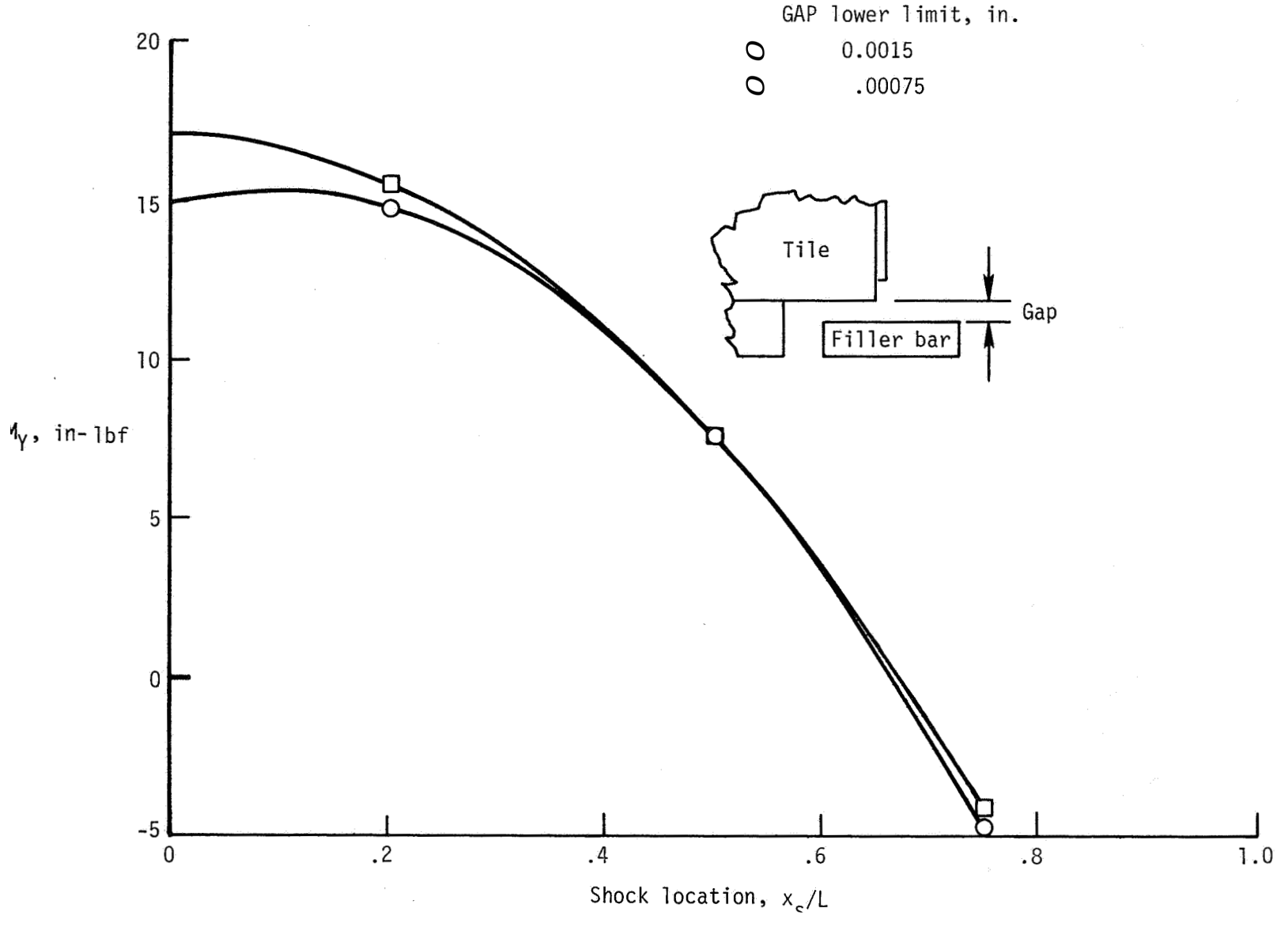

(a) Moment, gap between filler bar and tile, nominal lower limit, 0.001 in.

Figure 26.- Continued.

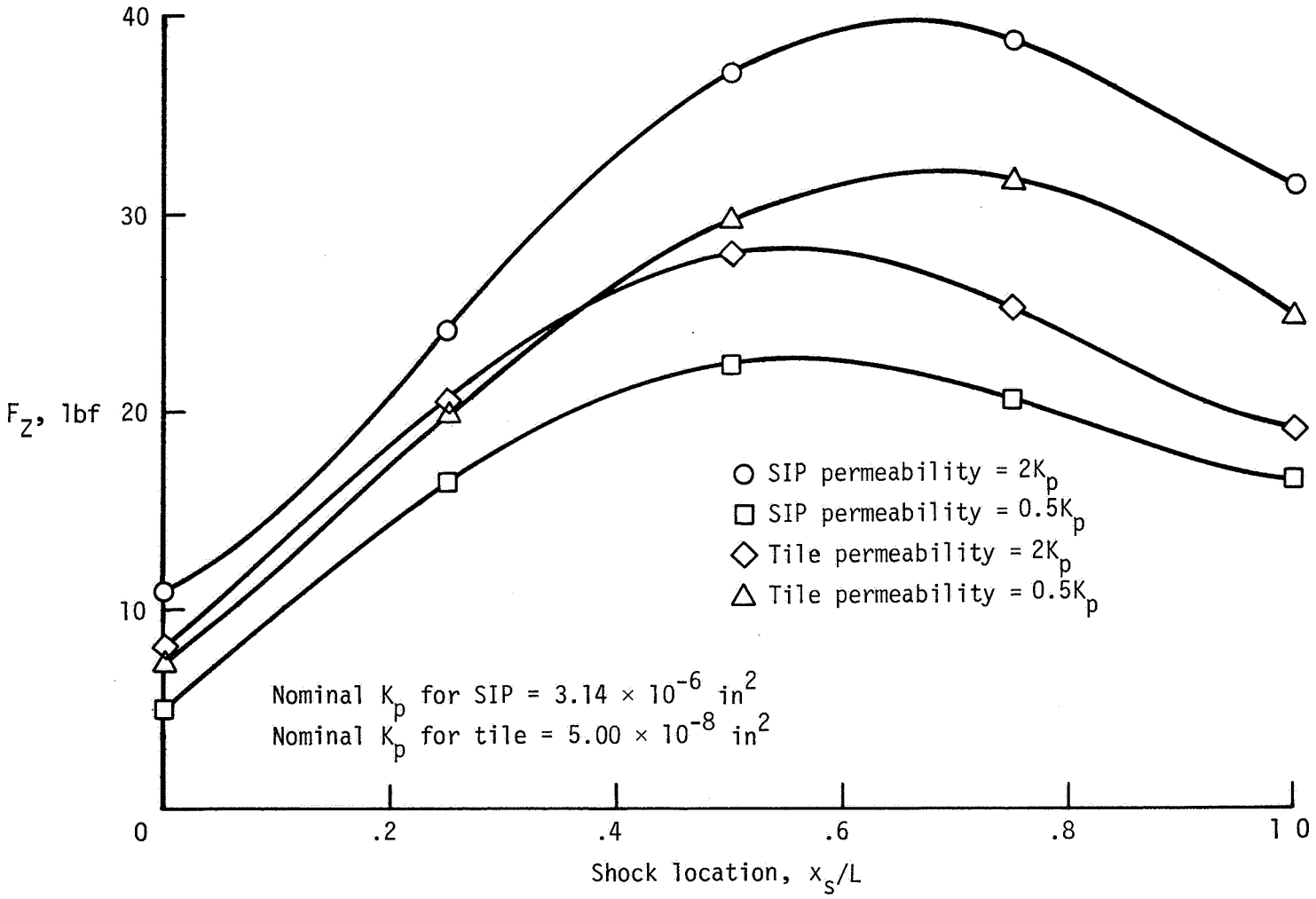

(e) Normal force; permeability.

Figure 26.- Continued.

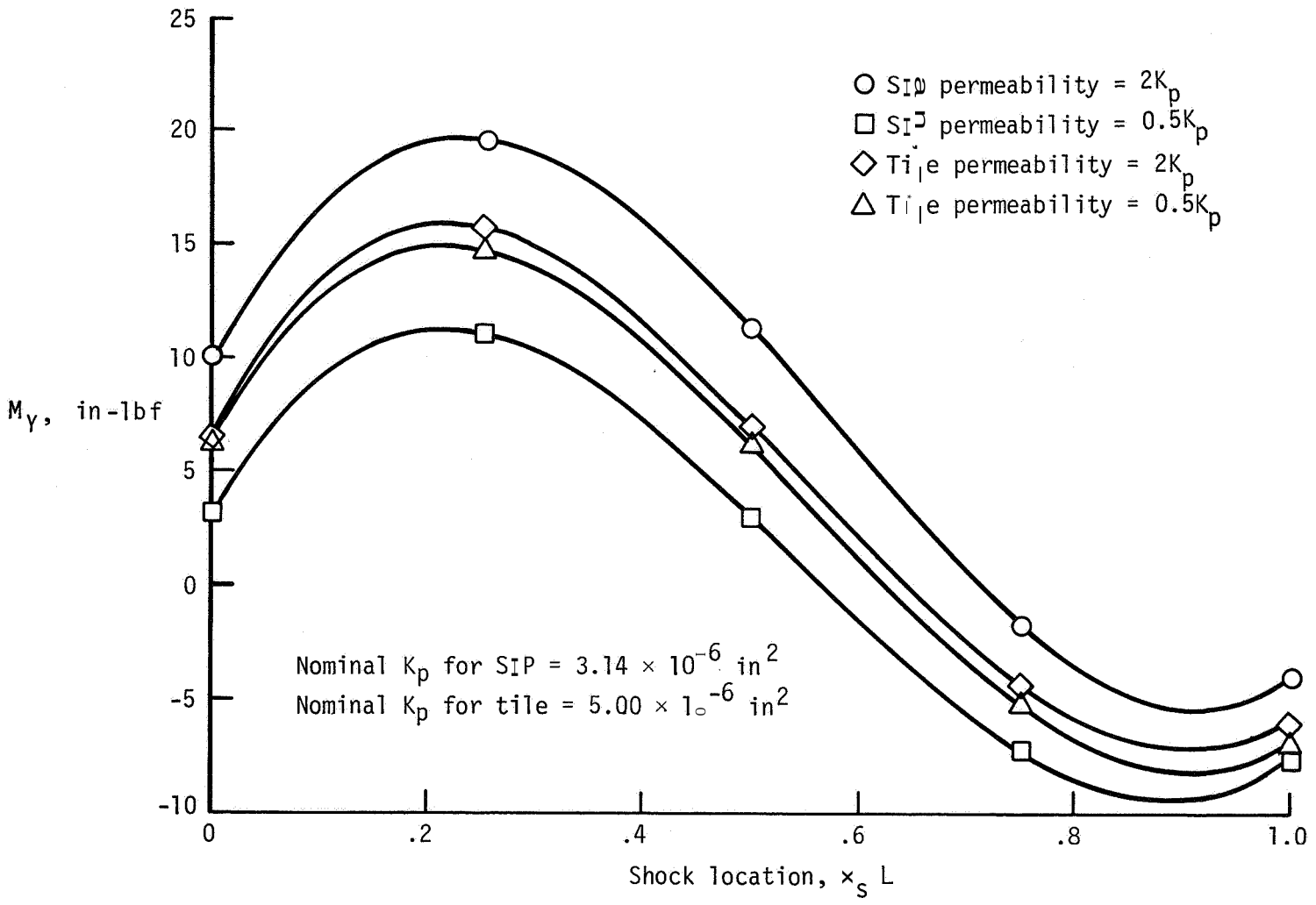

(f) Moment; permeability.

Figure 26.- Concluded.

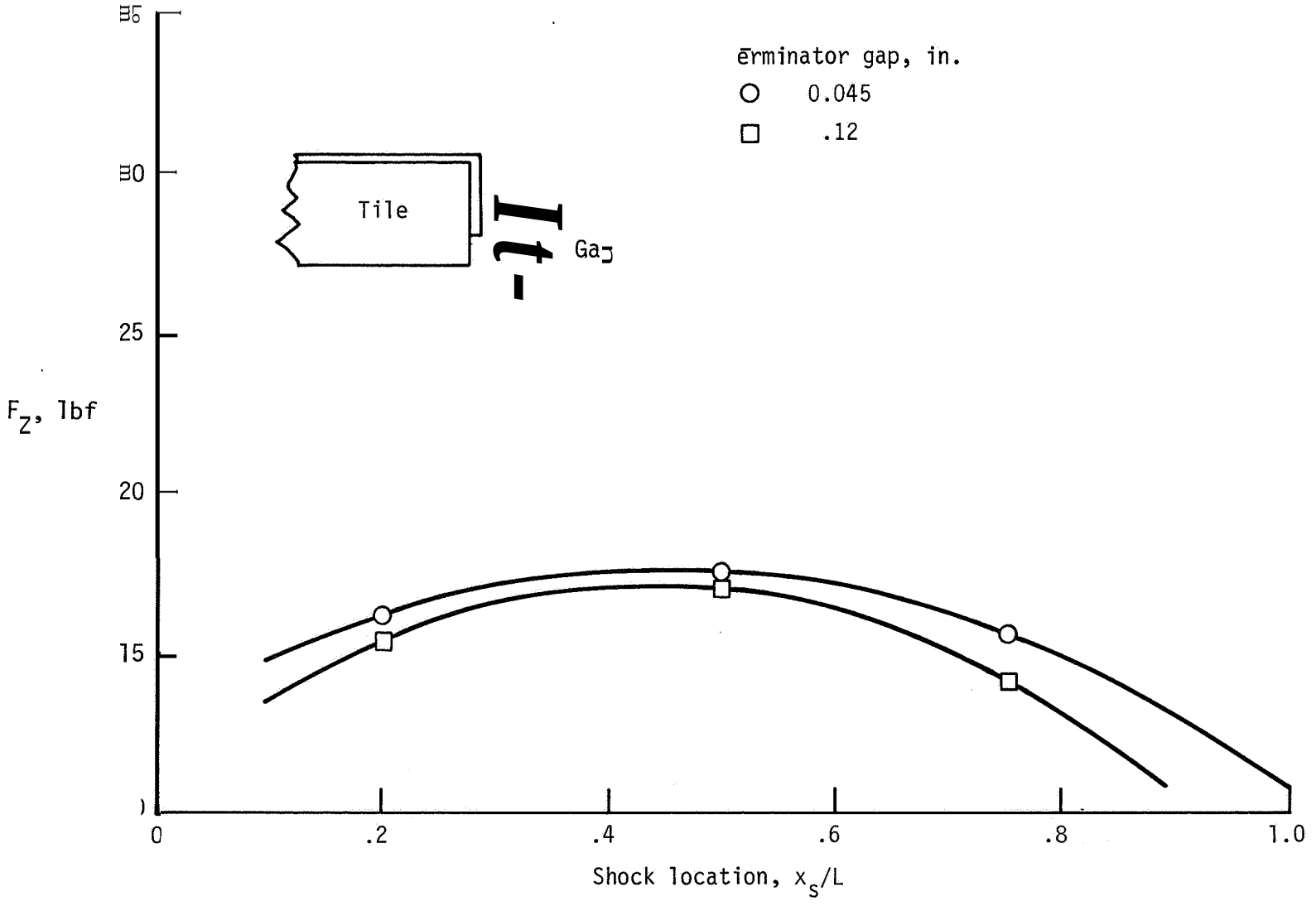

(a) rmal force; terminator gap.

Figure 27.- Calculated normal force and moment as function of shock location for MF-6 region, pressure profile B, separated shock, LI900 undensified tile 394034-087, and tile thickness of 1 in.

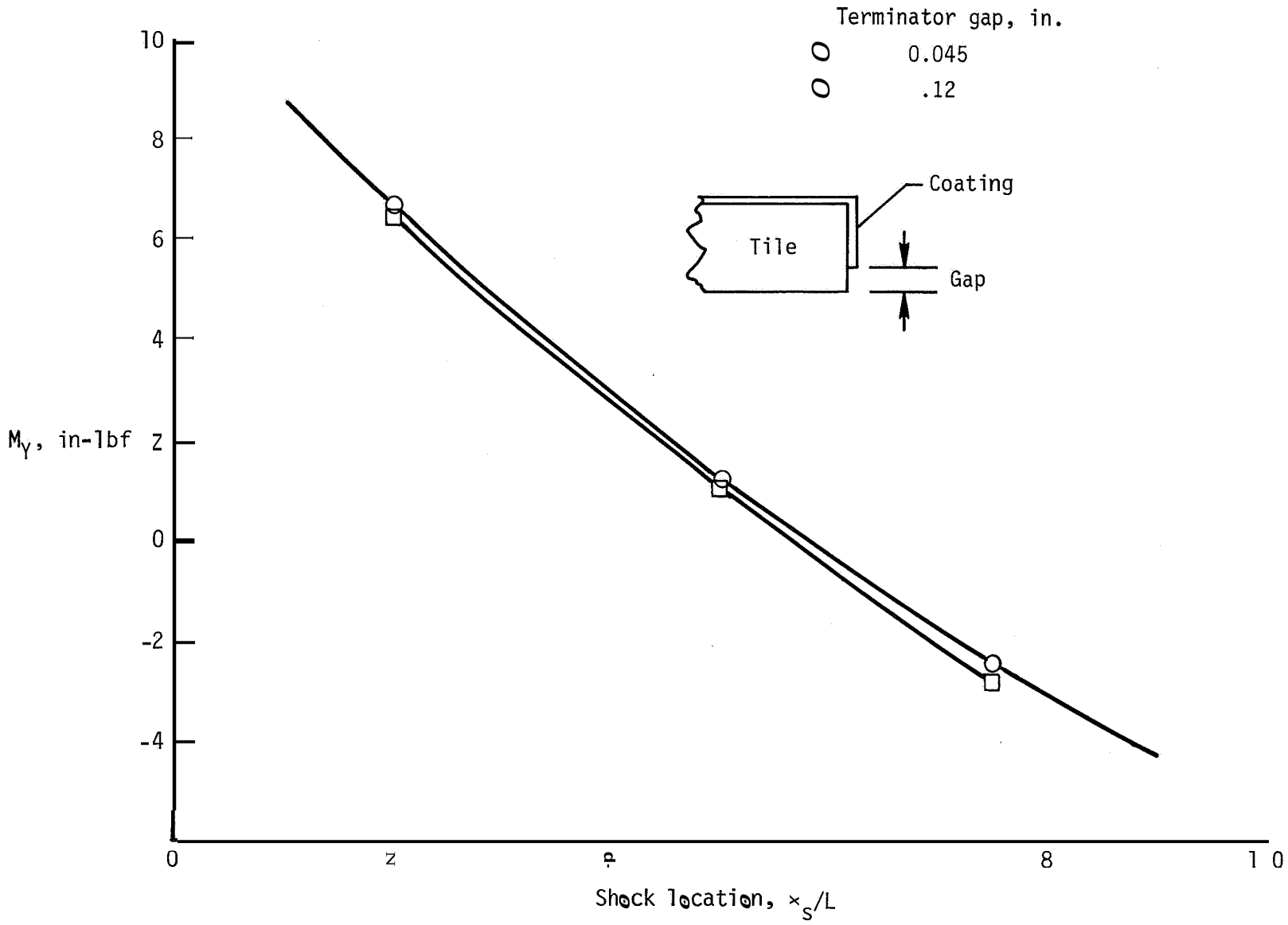

(b) Moment terminator gap.

Figure 27.- Continued.

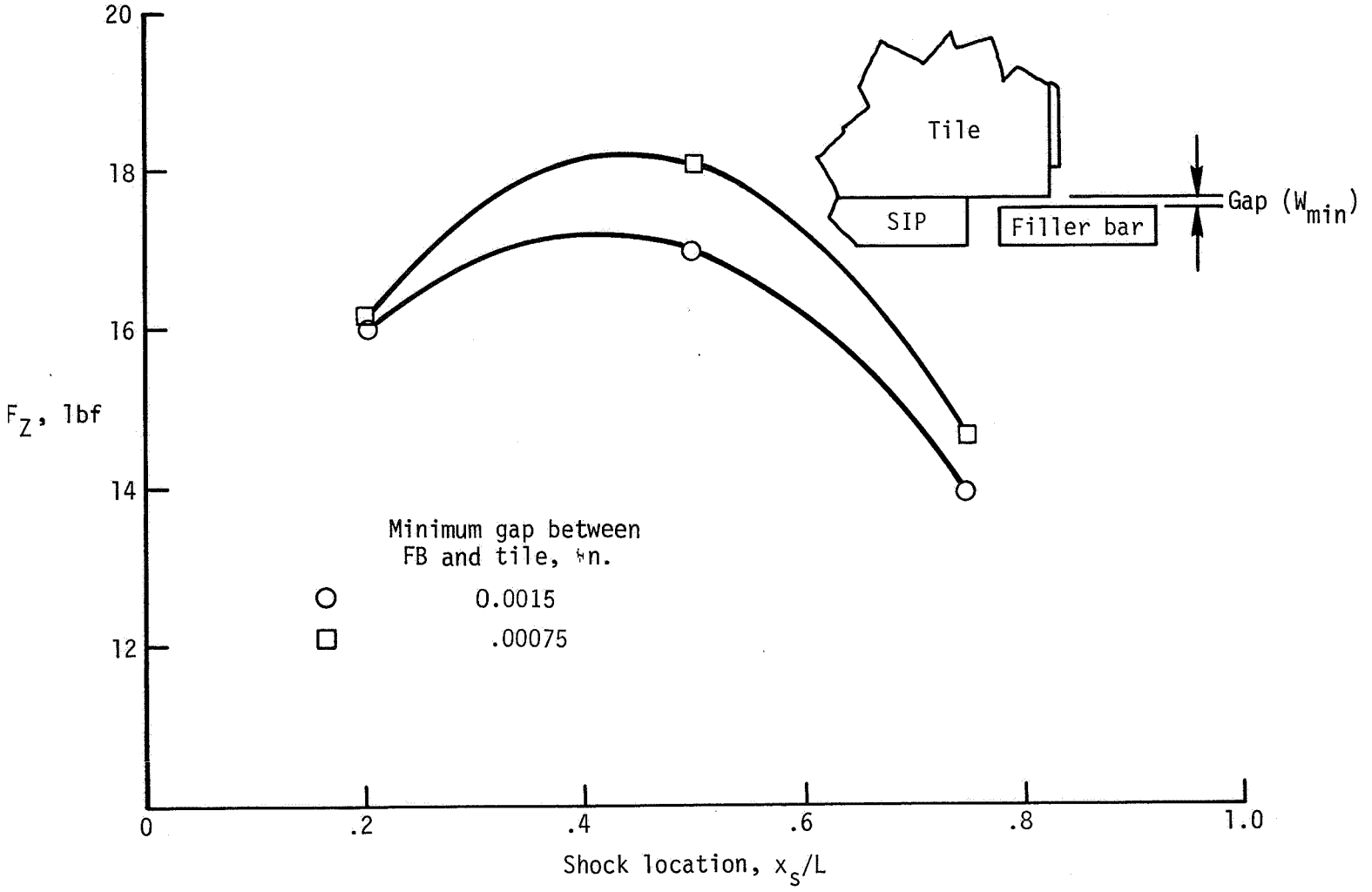

(c) Normal force, gap between filler bar and tile.

Figure 27.- Continued.

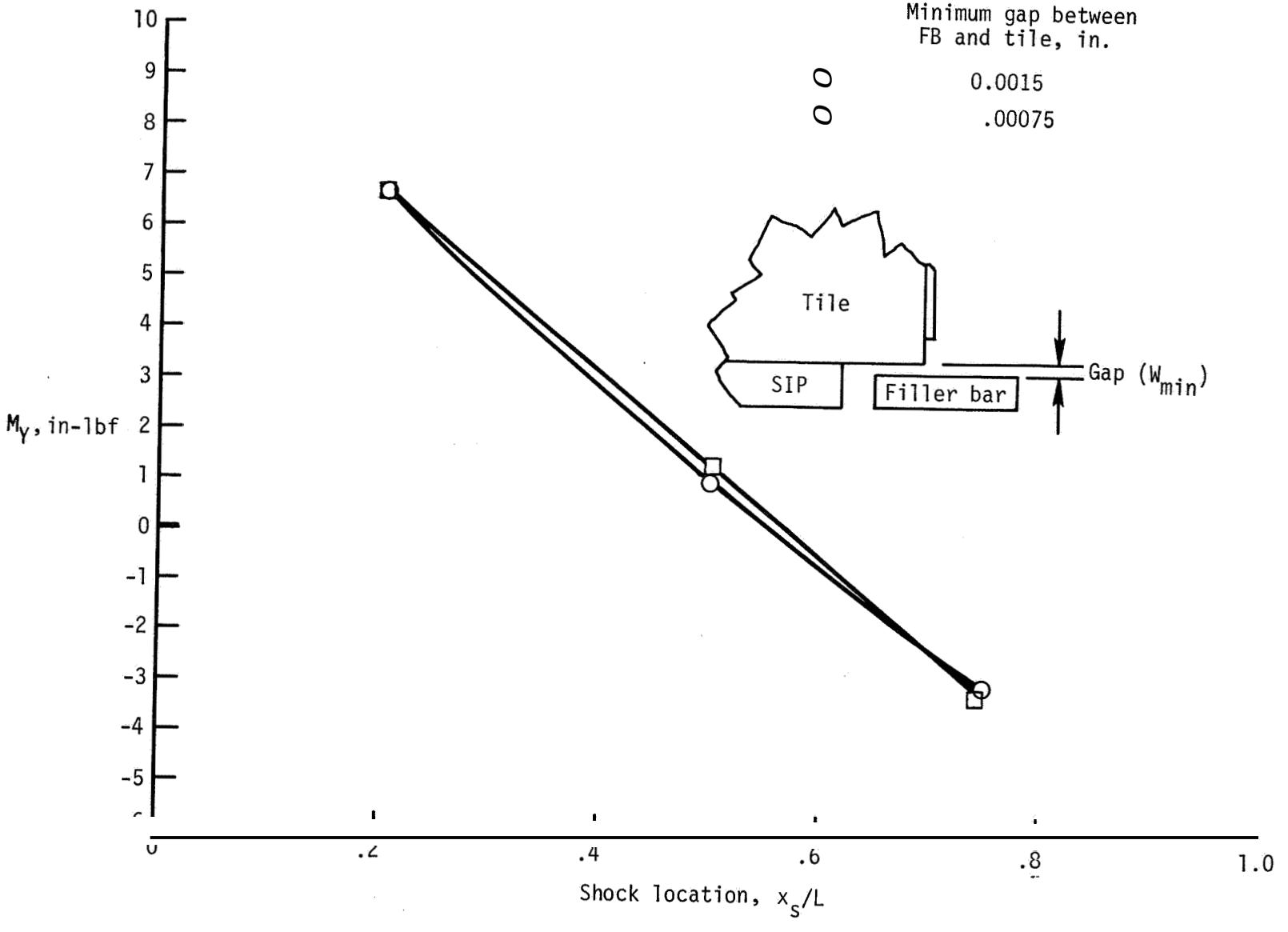

(d) Moment; gap between filler bar and tile.

Figure 27.- Concluded.

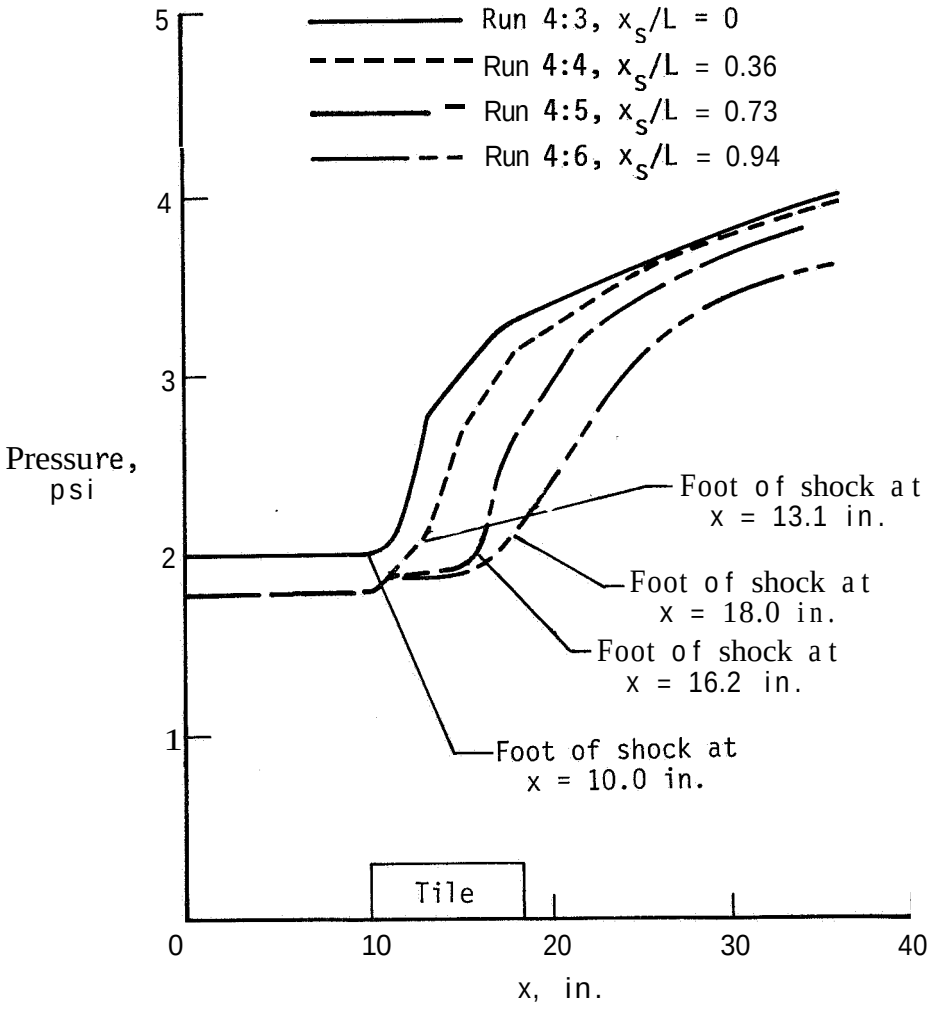

Figure 28.- Centerline pressure profiles for *OS55* and tile 45.

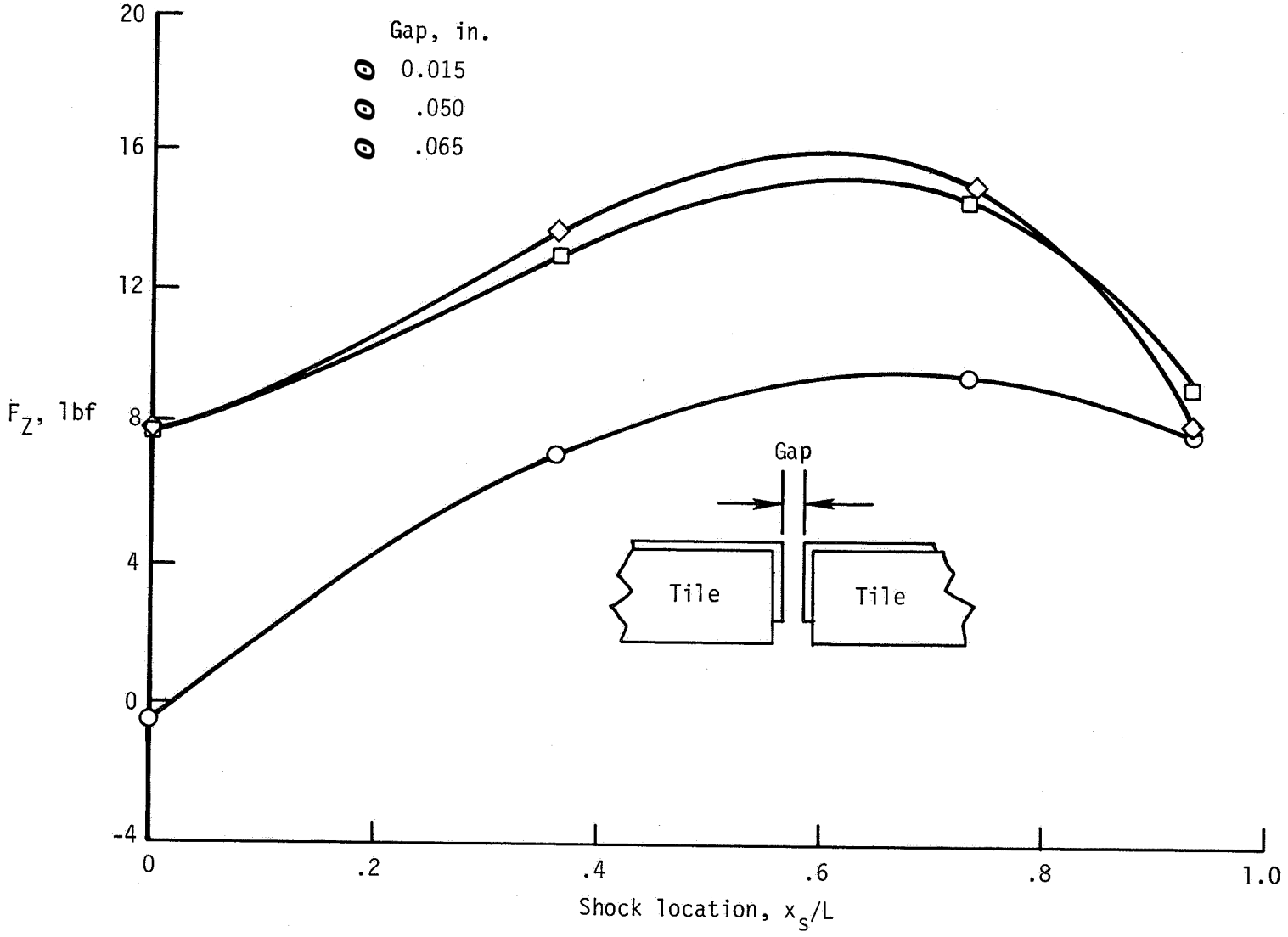

(a) Normal force.

Figure 29.- Calculated normal force and moment as function of shock location for OS55 pressure profile.

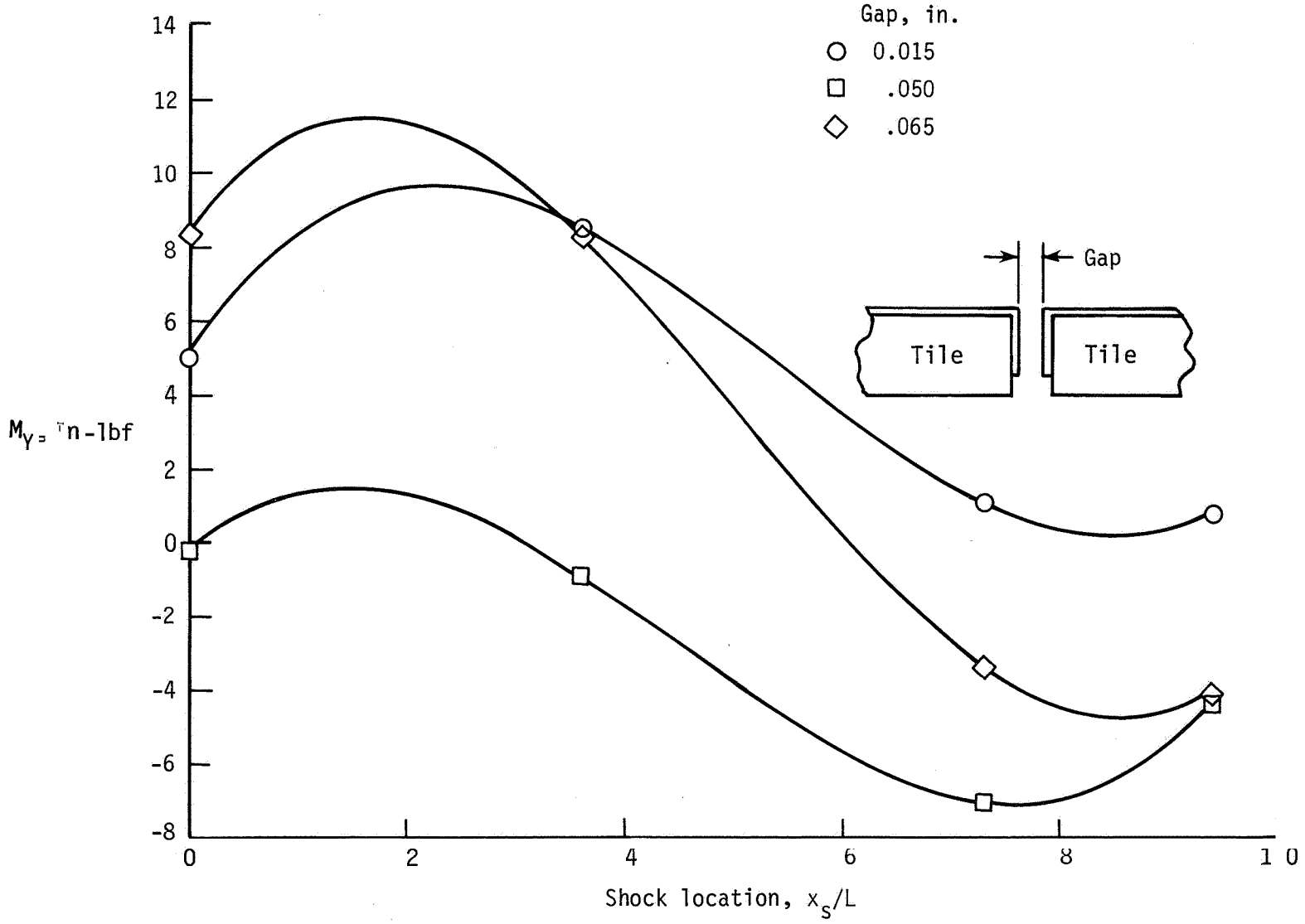

(b) Moment.

Figure 29.- Concluded.

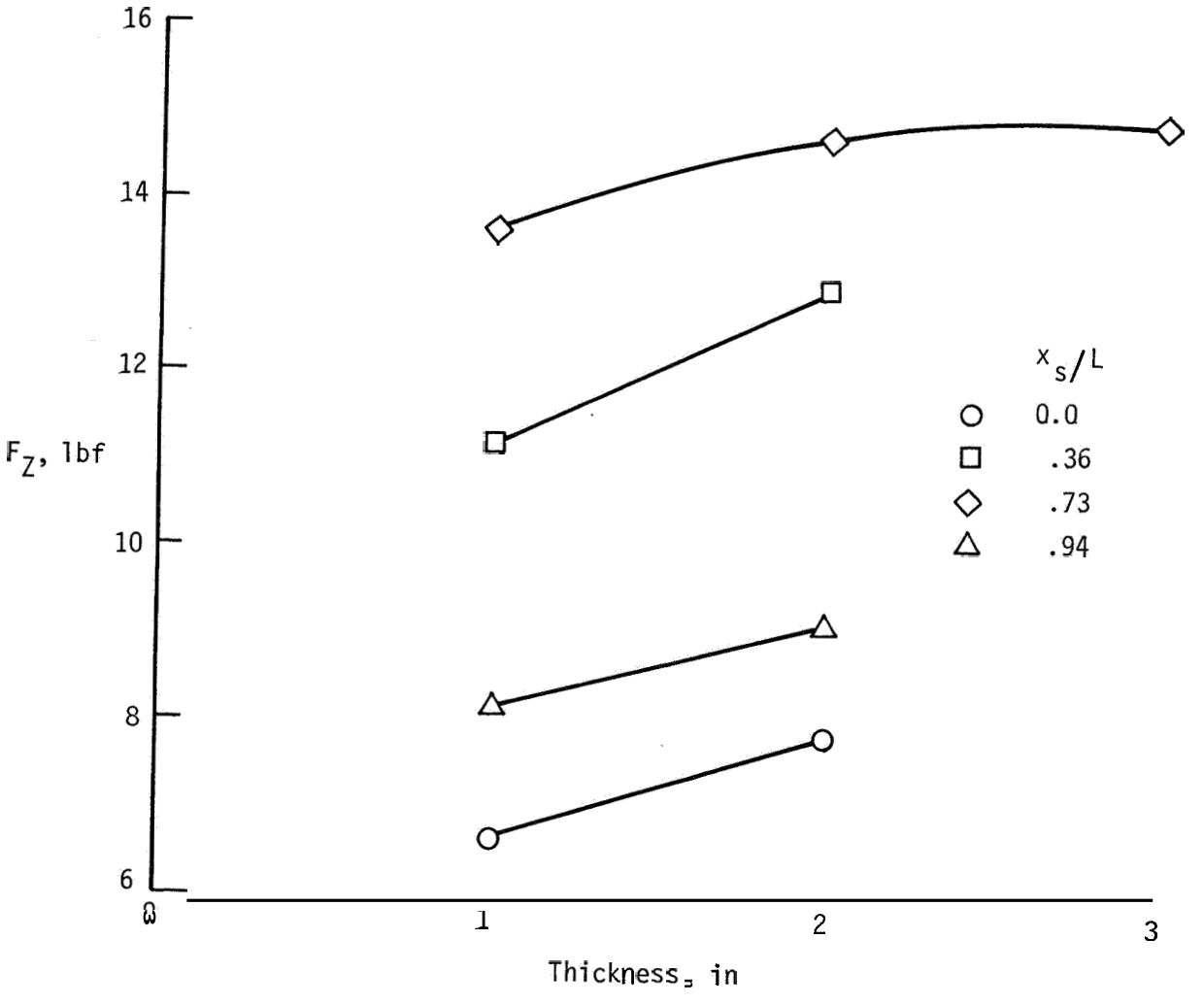

(a) Normal force.

Figure 30.- Calculated normal force and moment as function of thickness for OS55 pressure profile.

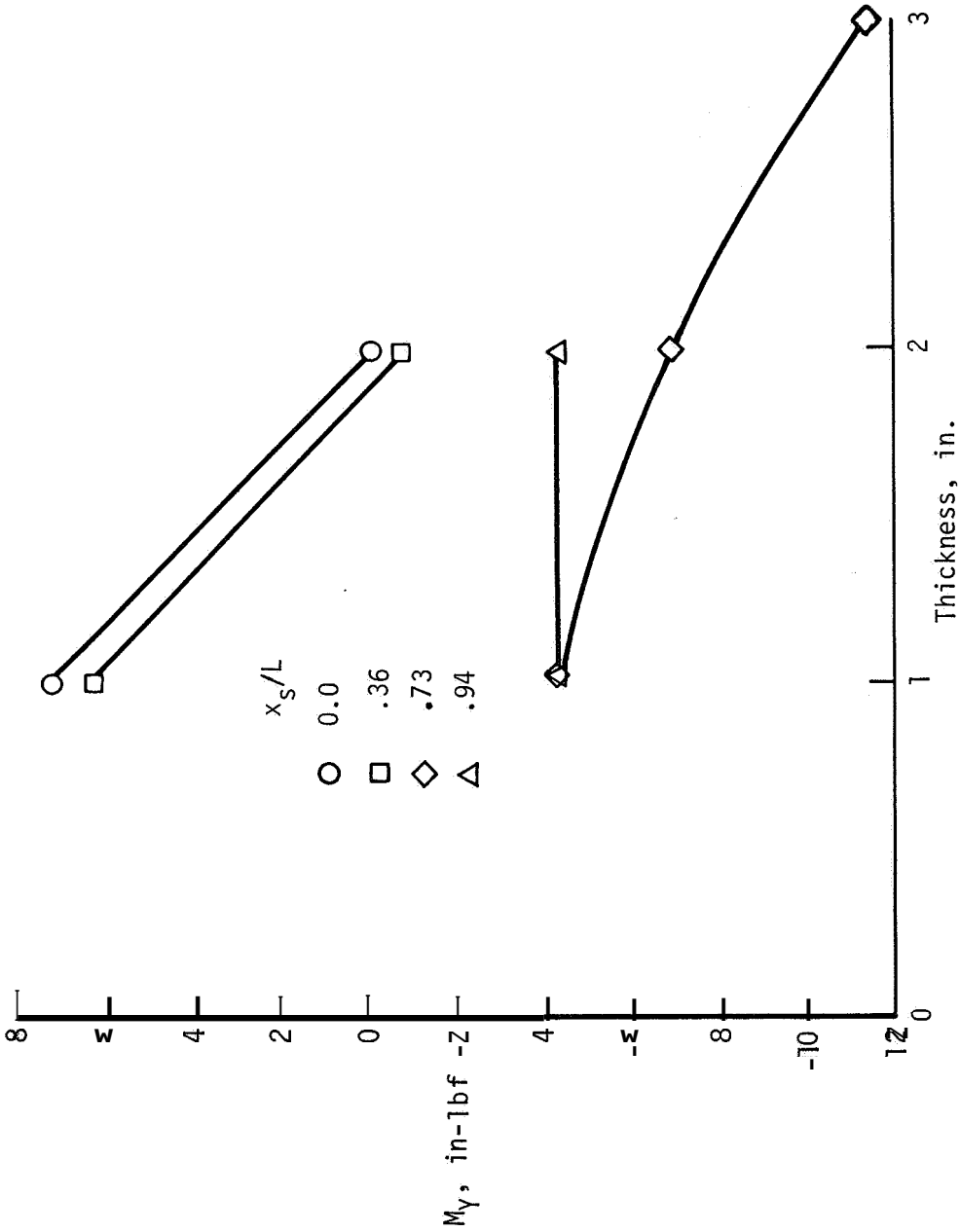

(b) Moment.

Figure 30.- Concluded.

1. Report No.	2. Government Accession No.	3. Recipient's Catalog No.
NASA TP-2255		

4. Title and Subtitle	5. Report Date
STEADY INTERNAL FLOW AND AERODYNAMIC LOADS ANALYSIS OF SHUTTLE THERMAL PROTECTION SYSTEM	March 1984
	6. Performing Organization Code 505-31-53-08
7. Author(s) Dennis H. Petley, William Alexander, Jr., George W. Ivey, Jr., and Patricia A. Kerr	8. Performing Organization Report No. L-15695
	10. Work Unit No.
9. Performing Organization Name and Address NASA Langley Research Center Hampton, VA 23665	11. Contract or Grant No.
	13. Type of Report and Period Covered Technical Paper
12. Sponsoring Agency Name and Address	14. Sponsoring Agency Code

15. Supplementary Notes

16. Abstract

An analytical model for calculation of ascent steady-state tile loading was developed and validated with wind-tunnel data. The analytical model is described and results are given. Results are given for loading due to shocks and skin friction. The analysis included calculation of internal flow (porous media flow and channel flow) to obtain pressures and integration of the pressures to obtain forces and moments on an insulation tile. A heat-transfer program was modified by using analogies between heat transfer and fluid flow so that it could be used for internal-flow calculation. The type of insulation tile considered was undensified reusable surface insulation (RSI) without gap fillers, and the location studied was the lower surface of the orbiter. Force and moment results are reported for parameter variations on surface pressure distribution, gap sizes, insulation permeability, and tile thickness.

17. Key Words (Suggested by Author(s))	18. Distribution Statement
Thermal Protection System Ascent loading from shock flow Internal incompressible flow Porous media Channel flow	Unclassified - Unlimited Subject Category 18

19. Security Classif. (of this report)	20. Security Classif. (of this page)	21. No. of Pages	22. Price
Unclassified	Unclassified	67	A04

For sale by the National Technical information Service, Springfield, Virginia 22161 NASA-Langley, 1984